

Testing the Gaussian Approximation to the JIMWLK Equation

M. Alvioli*

European Centre for Theoretical Studies in Nuclear Physics and Related Areas (ECT),
Strada delle Tabarelle 286, I-38123 Villazzano (TN), Italy*

G. Soyez†

Institut de Physique Théorique, CEA/Saclay, F-91191 Gif-sur-Yvette, France

D.N. Triantafyllopoulos‡

European Centre for Theoretical Studies in Nuclear Physics and Related Areas (ECT)
and Fondazione Bruno Kessler, Strada delle Tabarelle 286, I-38123 Villazzano (TN), Italy*

(Dated: February 6, 2013)

In processes involving small- x partons, like in deep inelastic scattering and in hadronic collisions at high energy, the final state can be expressed in terms of correlators of Wilson lines. We study such high-point correlators evolving according to the JIMWLK equation and we confirm the results of previous numerical and analytic work, by using an independent method, that the solution to the JIMWLK equation can be very well approximated by an appropriate Gaussian wavefunction. We explore both fixed and running coupling evolution, where in the latter the scale is set according to various prescriptions. As a byproduct, we also numerically confirm to high accuracy the validity of the law governing the behavior of the S -matrix close to the unitarity limit, the Levin-Tuchin formula. We furthermore outline how to calculate correlators with open color indices.

PACS numbers: 12.38.Mh, 12.38.Bx, 25.75.-q

* alvioli@pg.infn.it; Current affiliation: *CNR-IRPI, via Madonna Alta 126, I-06128 Perugia (PG), Italy*

† gregory.soyez@cea.fr

‡ trianta@ectstar.eu

I. INTRODUCTION AND MOTIVATION

In hadronic collisions at ultra-relativistic energies the final state is quite involved in terms of the type, the number and the distribution of the produced particles. The extraction of the dominant physical mechanisms in such processes is a demanding task and in order to achieve the best possible understanding it is necessary to study many observables in wide kinematic regimes. For instance, significant attention has been given to collisions between light and heavy hadrons, like deuteron-gold at RHIC and the forthcoming proton-lead at the LHC and in both cases two of the most representative observables are related to single and double inclusive particle production. Considering the single inclusive particle production in the deuteron fragmentation region it has been observed, already a few years ago at RHIC [1, 2], a suppression compared to the cross section obtained by taking the nucleus as an incoherent superposition of $A^{1/3}$ nucleons. More recently, and regarding the double inclusive particle production, it has been seen an increasing suppression of the azimuthal correlation of the two hadrons when their transverse momenta are a few GeV [3, 4], as we move towards the deuteron fragmentation region.

This is precisely the kinematic regime which encourages the search for parton saturation in the wave-function of the heavy hadron, the large nucleus. Natural qualitative and quantitative descriptions of the RHIC data and predictions for the LHC upcoming ones based on such a physical mechanism, along with the corresponding formulations, already exist for the nuclear modification factor R_{pA} [5–16], which is related to the single inclusive cross section. Similarly, the di-hadron azimuthal correlations at RHIC offer a unique environment to test parton saturation [17, 18] and in fact the corresponding data have been understood in that context [19–22].

Thus, one is particularly interested in $hA \rightarrow h'X$ and $hA \rightarrow h_1h_2X$, with h a projectile hadron whose wavefunction is not saturated, like a proton at not too high energy so that its small- x evolution can be neglected, and A a target who can be dense, like an ultra-relativistic heavy nucleus. Let us again look at single particle production first for which the corresponding diagram at the partonic level, say for quark production, is shown in Fig. 1.(a). A large- x quark from the projectile interacts via multiple gluon exchanges with the small- x components of the target and then it is measured in the region which is forward in (pseudo)rapidity. The target is viewed as a potentially large color field \mathcal{A}_a^μ , the Color Glass Condensate (CGC) (see e.g. [23]) and the interaction of a parton with transverse position \mathbf{x} with such a field is described by a Wilson line along its trajectory. Taking the modulus squared of the diagram 1.(a) in coordinate space, averaging over initial colors and summing over final ones, we find the cross section $qA \rightarrow qX$ to be given by the Fourier transform of a color dipole \hat{S} , that is, a trace of two Wilson lines in the fundamental representation, which is an overall colorless object.

The above discussion naturally extends to the case of double particle production when both particles are detected at the same rapidities. Without any loss of generality, let us focus on qq production¹ at the partonic level with the respective diagrams shown in Fig. 1.(b) and (c). The large- x projectile quark splits into a quark-gluon pair, and this splitting can occur either before

¹ Here and in the previous paragraph, we discuss only representative cases of single and double inclusive particle production which are taken to be quark and quark-gluon production respectively. Other possibilities like gluon and gluon-pair production have been also studied and understood [17, 24–28].

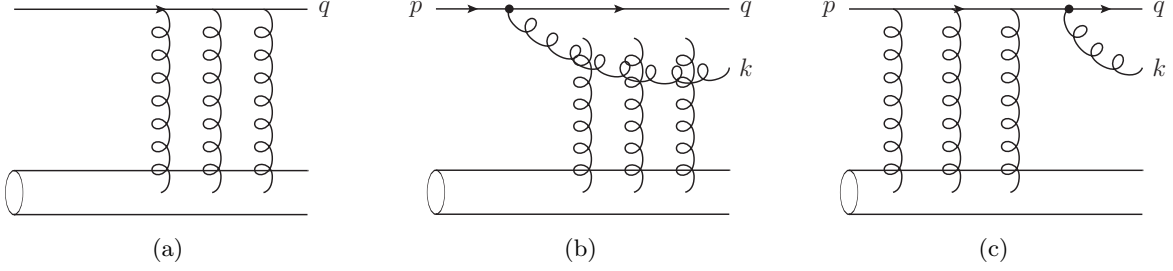


FIG. 1. (a) Quark production and (b), (c) quark-gluon production in pA collisions.

or after the interaction with the target. Now one arrives at an inclusive $qA \rightarrow qgX$ cross section [18] which is given by a Fourier transform of various terms involving two, four or six Wilson lines. Such a term with the maximal number of Wilson lines is $\hat{S}\hat{Q}$, that is, a color dipole times a color quadrupole, where the latter is a trace of four Wilson lines, and in fact it is not hard to understand the counting of Wilson lines. For instance, diagram (b) involves one in the fundamental and one in the adjoint representation and the latter can be expressed in terms of two fundamental ones. When multiplied with its complex conjugate it gives rise to the aforementioned $\hat{S}\hat{Q}$ term which involves six Wilson lines (plus a $1/N_c^2$ correction). Clearly, one realizes that the production of more and more particles at forward rapidities will involve more and more Wilson lines. Interestingly enough, it was recently shown that in the large- N_c limit any forward multi-particle production cross section can be expressed only in terms of dipoles and quadrupoles [29].

Thus, in general, one needs to calculate correlators of the form $\langle \hat{O} \rangle_Y$, where \hat{O} is constructed from such multipoles. Obviously the Wilson lines depend on the target field and the average has to be taken with the target probability distribution $W_Y[\mathcal{A}]$, which simply gives the probability to find a given configuration in the target wavefunction. The rapidity Y is determined by the kinematics of the process under consideration; for example, for qg production at forward rapidities one has $x = \exp(-Y) = [|\mathbf{k}| \exp(-|y_k|) + |\mathbf{q}| \exp(-|y_q|)]/\sqrt{s}$, with \mathbf{q} and y_q the transverse momentum and (pseudo)rapidity of the produced quark, \mathbf{k} and y_k those of the gluon and \sqrt{s} the center of mass energy. At moderately small values of x one typically invokes the McLerran-Venugopalan (MV) model [30, 31], which is equivalent to a Gaussian wavefunction $W_Y[\alpha]$ and thus allows for explicit calculation of high-point correlators [17, 32, 33].

As we move towards higher values of y_q and y_k , we probe components of the target with smaller- x and it becomes necessary to take into account the evolution in Y of $W_Y[\mathcal{A}]$. Even though this is a classical probability distribution its evolution is quantum and satisfies the JIMWLK equation [34–38] which arises from the resummation of the dominant terms in $\ln(1/x)$ in the presence of a potentially strong color field. Using the Langevin form of the JIMWLK equation [39], a critical work on its numerical solution was recently performed, where the very good accuracy of a particular Gaussian approximation, the extension to arbitrary Y of the MV model, was observed for some configurations of high-point correlators [40]. Immediately after it was analytically understood why the approximation scheme based on a Gaussian wavefunction provides a quasi-exact solution to the JIMWLK equation [41, 42].

Our effort, which is mostly numerical, may be considered as complementary to the work in [40]

to some extent, but it is completely independent for a number of reasons. (i) The method here is different; instead of studying JIMWLK as a Langevin equation on a lattice, we directly analyze evolution equations for given configurations. But even if one starts from a simple configuration, evolution always creates more general ones (cf. Figs. 8 and 9) and eventually our tests probe a much wider sample. (ii) We shall explore a larger kinematical space and as a byproduct we shall be able to give a numerical verification of the Levin-Tuchin formula [43] (see also [44–47]). (iii) We will study both fixed and running coupling evolution, where the scheme in the latter case can be chosen at our will. (iv) We can consider any value for the number of colors N_c , even though we shall mainly work in the multicolor limit.

The paper is mostly devoted to technical aspects concerning the validity of a certain approximation scheme and its structure is the following: In Sect. II we review the JIMWLK equation and how it determines the evolution of multi-parton correlations. In this Section we also introduce most of our definitions along with the corresponding notation. In Sect. III we give an accurate numerical solution to the Balitsky-Kovchegov (BK) equation, that is, the large- N_c equation for the dipole [48, 49]. In particular we focus on the regime where saturation has been reached, a necessary step for our purposes, and we verify for the first time the validity of the Levin-Tuchin formula. Moreover, from the form of the solution at saturation, we also confirm the two most dominant terms in the asymptotic expansion of the saturation momentum Q_s for fixed coupling evolution. In Sect. IV we briefly reflect on the Gaussian approximation and why it is expected to work accurately [41, 42]. In Sect. V we study numerically a Mean Field Equation arising from the Gaussian approximation to the JIMWLK Hamiltonian and show that it is in agreement with the BK equation to logarithmic accuracy at saturation as expected. In Sect. VI we examine two quadrupole configurations and show, for both fixed and running coupling evolution (the latter in the Balitsky, smallest dipole and daughter dipole prescriptions), that the accuracy is not restricted to be logarithmic, giving further evidence that the Gaussian approximation is a “quasi-exact” solution. We point out a potential deficiency of a “too simple” Gaussian approximation (in particular the extrapolation to arbitrary Y of the MV model) in the running coupling case and at saturation, but it seems not to be crucial for practical purposes. In Sect. VII we outline how one can calculate correlators with open color indices and finally in Sect. VIII we conclude.

II. THE JIMWLK EQUATION AND MULTI-PARTON CORRELATIONS

The Color Glass Condensate (CGC) is a modern effective theory for the small- x components of the wavefunction of an ultra-relativistic hadron. It relies on the idea that gluons which carry a small fraction x of the hadron’s longitudinal momentum can be described as a random distribution of classical color fields generated by sources with larger momentum fractions. As a result of the high energy kinematics, the distribution of the color sources is frozen due to Lorentz time dilation and the color field, in a suitable gauge, has a single non-zero component. More precisely, and using the standard definitions for the light-cone coordinates $x^\mu = (x^+, x^-, \mathbf{x})$, with $x^\pm = (t \pm x^3)/\sqrt{2}$ and $\mathbf{x} = (x^1, x^2)$, this gauge field is $\mathcal{A}_a^\mu(x) = \delta^{\mu+} \alpha_a(x^-, \mathbf{x})$ if the hadron moves along the positive x^3 -axis. The CGC weight function $W_Y[\alpha]$ gives the probability that the hadron be described by

the configuration α and it is a functional probability distribution whose knowledge allows the determination of the correlations of the gauge field. The latter contain all the detailed information about the evolution of the hadron with increasing rapidity $Y \equiv \ln(1/x)$, from an initial value $Y_0 = \ln(1/x_0)$ to the value Y of interest. At high energy where $\alpha_s(Y - Y_0) \gtrsim 1$ and to leading order with respect to the large logarithm $\ln(x_0/x)$, this evolution obeys a renormalization group equation, the JIMWLK equation [34–38]. In a Hamiltonian form it reads

$$\frac{\partial}{\partial Y} W_Y[\alpha] = H W_Y[\alpha], \quad (2.1)$$

where H is the JIMWLK Hamiltonian and it is a second-order functional differential operator whose most elegant and convenient for our purposes form was given is [50]

$$H = -\frac{1}{16\pi^3} \int_{\mathbf{uvz}} \mathcal{M}_{\mathbf{uvz}} \left(1 + \tilde{V}_{\mathbf{u}}^\dagger \tilde{V}_{\mathbf{v}} - \tilde{V}_{\mathbf{u}}^\dagger \tilde{V}_{\mathbf{z}} - \tilde{V}_{\mathbf{z}}^\dagger \tilde{V}_{\mathbf{v}} \right)^{ab} \frac{\delta}{\delta \alpha_{\mathbf{u}}^a} \frac{\delta}{\delta \alpha_{\mathbf{v}}^b}. \quad (2.2)$$

Here we have used the economical notation $\int_{\mathbf{u}\dots} \equiv \int d^2\mathbf{u} \dots$, defined the dipole kernel \mathcal{M} [51]

$$\mathcal{M}_{\mathbf{uvz}} \equiv \frac{(\mathbf{u} - \mathbf{v})^2}{(\mathbf{u} - \mathbf{z})^2 (\mathbf{z} - \mathbf{v})^2} \quad (2.3)$$

and introduced the Wilson lines

$$\tilde{V}_{\mathbf{x}}^\dagger \equiv \text{P exp} \left[ig \int dx^- \alpha_a(x^-, \mathbf{x}) T^a \right], \quad (2.4)$$

where T^a is in the adjoint representation and with P denoting path-ordering in x^- . The precise action of the functional derivatives appearing in Eq. (2.2) will be explained later on. The above form of the Hamiltonian is valid only when acting on gauge-invariant functionals of α_a , like gauge-invariant products of Wilson lines. This will be the case for most of our analysis with exceptions to be discussed at the end in Sect. VII. Needless to say, in order to specify our problem completely, we need an initial condition for Eq. (2.1) at $Y = Y_0$. At least for a sufficiently large nucleus ($A \gg 1$, with A the atomic mass number), this initial condition is typically provided by the McLerran-Venugopalan (MV) model [30, 31].

Physical observables are represented by gauge invariant operators $\hat{\mathcal{O}}[\alpha]$ constructed with the gauge color field α_a . Their expectation value can be computed as a functional average with the CGC weight function, that is

$$\langle \hat{\mathcal{O}} \rangle_Y \equiv \int \mathcal{D}\alpha \mathcal{O}[\alpha] W_Y[\alpha]. \quad (2.5)$$

The above makes clear that, even though $W_Y[\alpha]$ is obtained by a quantum calculation, the averaging procedure is classical. Differentiating the above with respect to Y , using Eq. (2.1), and finally integrating twice by parts, we arrive at the evolution equation

$$\frac{\partial \langle \hat{\mathcal{O}} \rangle_Y}{\partial Y} = \langle H \hat{\mathcal{O}} \rangle_Y \quad (2.6)$$

for the observable under consideration. This is not a functional equation anymore, but an integro-differential equation as we shall see in a while in specific examples. Still, this is not much easier

to deal with since, due to the non-linear dependence of the Hamiltonian (2.2) on the field α_a , Eq. (2.6) is in general not a closed equation, but just a member of an infinite hierarchy of coupled equations, the Balitsky equations [48, 52]. The JILWLK equation (2.1) and the Balitsky hierarchy offer complementary views on the high-energy evolution. On the one hand, Eq. (2.1) describes the evolution of the target by the emission of an additional gluon with rapidity between Y and $Y + dY$ in the background of the gauge color field α built by previous emissions, at rapidities smaller than Y . The Wilson lines in the Hamiltonian (2.2) correspond to the propagation of this new gluon in the background field and in the eikonal approximation. On the other hand, the Balitsky hierarchy focuses on the projectile evolution and in particular on the operator describing its scattering off the target. This scattering is again considered in the eikonal approximation and therefore the operator $\hat{\mathcal{O}}$ is naturally constructed with Wilson lines, where each one of them represents a parton in the projectile.

We shall mostly focus on the color dipole made by a quark-antiquark pair in an overall color singlet state, with the S -matrix

$$\hat{S}_{\mathbf{x}_1 \mathbf{x}_2} \equiv \hat{S}_{\mathbf{x}_1 \mathbf{x}_2}^{(2)} = \frac{1}{N_c} \text{tr}(V_{\mathbf{x}_1}^\dagger V_{\mathbf{x}_2}), \quad (2.7)$$

and the color quadrupole, a system of two quarks and two antiquarks also in a color singlet, for which

$$\hat{Q}_{\mathbf{x}_1 \mathbf{x}_2 \mathbf{x}_3 \mathbf{x}_4} \equiv \hat{S}_{\mathbf{x}_1 \mathbf{x}_2 \mathbf{x}_3 \mathbf{x}_4}^{(4)} = \frac{1}{N_c} \text{tr}(V_{\mathbf{x}_1}^\dagger V_{\mathbf{x}_2} V_{\mathbf{x}_3}^\dagger V_{\mathbf{x}_4}). \quad (2.8)$$

Here V^\dagger and V are Wilson lines like in Eq. (2.4), but in the fundamental representation. In general one can consider projectiles made with n quarks and n antiquarks, for which

$$\hat{S}_{\mathbf{x}_1 \mathbf{x}_2 \dots \mathbf{x}_{2n-1} \mathbf{x}_{2n}}^{(2n)} = \frac{1}{N_c} \text{tr}(V_{\mathbf{x}_1}^\dagger V_{\mathbf{x}_2} \dots V_{\mathbf{x}_{2n-1}}^\dagger V_{\mathbf{x}_{2n}}), \quad (2.9)$$

and eventually high energy evolution mixes such single-trace operators with multi-trace ones of the form

$$\hat{\mathcal{O}} = \frac{1}{N_c} \text{tr}(V_{\mathbf{x}_1}^\dagger V_{\mathbf{x}_2} \dots) \frac{1}{N_c} \text{tr}(V_{\mathbf{y}_1}^\dagger V_{\mathbf{y}_2} \dots) \frac{1}{N_c} \text{tr}(V_{\mathbf{z}_1}^\dagger V_{\mathbf{z}_2} \dots). \quad (2.10)$$

The quadrupole defined above in Eq. (2.8) is the first non-trivial operator which can probe multi-parton correlation in the target wavefunction and will serve as the prototype in our study. In order to construct evolution equations according to Eqs. (2.2) and (2.6), it is necessary to specify how the functional derivatives w.r.t. α_a act on observables. They act on endpoints of the Wilson lines according to

$$\frac{\delta}{\delta \alpha_u^a} V_{\mathbf{x}}^\dagger = ig \delta_{\mathbf{x}u} t^a V_{\mathbf{x}}^\dagger, \quad \frac{\delta}{\delta \alpha_u^a} V_{\mathbf{x}} = -ig \delta_{\mathbf{x}u} V_{\mathbf{x}} t^a, \quad (2.11)$$

with t^a in the fundamental representation and where we introduced the shorthand notation $\delta_{\mathbf{x}u} = \delta^{(2)}(\mathbf{x} - \mathbf{u})$. Because of their action on V^\dagger (by convention), they are called “left” derivatives and could be also denoted as $\delta/\delta \alpha_L^a$. Using these rules within Eqs. (2.2) and (2.6), it is straightforward

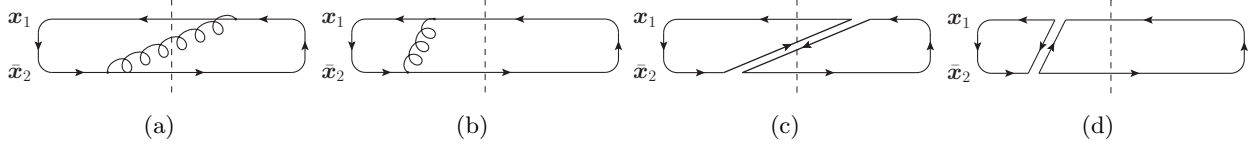


FIG. 2. (a) A real emission of a gluon from a color dipole. (b) A virtual emission. (c) and (d) The corresponding diagrams in the large- N_c limit. In all diagrams the dashed line stands for the interaction with the target.

to derive the evolution equations satisfied by the S -matrices for the dipole and the quadrupole. The resulting equation for the dipole is

$$\frac{\partial \langle \hat{S}_{\mathbf{x}_1 \mathbf{x}_2} \rangle_Y}{\partial Y} = \frac{\bar{\alpha}}{2\pi} \int_{\mathbf{z}} \mathcal{M}_{\mathbf{x}_1 \mathbf{x}_2 \mathbf{z}} \langle \hat{S}_{\mathbf{x}_1 \mathbf{z}} \hat{S}_{\mathbf{z} \mathbf{x}_2} - \hat{S}_{\mathbf{x}_1 \mathbf{x}_2} \rangle_Y, \quad (2.12)$$

where we have defined $\bar{\alpha} = \alpha_s N_c / \pi$. Even though derived by evolving the target, this equation has an easy interpretation in terms of projectile evolution, as shown in Fig. 2. The quadratic term in \hat{S} has been generated by the real part of the Hamiltonian H_{real} , that is, by the last two terms in the parenthesis in Eq. (2.2). It describes the splitting of the original dipole $(\mathbf{x}_1, \mathbf{x}_2)$ into two new dipoles $(\mathbf{x}_1, \mathbf{z})$ and $(\mathbf{z}, \mathbf{x}_2)$, which subsequently scatter off the target. More precisely, the evolution step consists of the emission of a soft gluon, hence the original dipole gets replaced by a quark-antiquark-gluon system, but in the large- N_c limit this emission is equivalent to the aforementioned dipole splitting. The negative, linear in \hat{S} , term has been produced by the virtual part of the Hamiltonian H_{virt} , that is, by the first two terms in the parenthesis in Eq. (2.2) and corresponds to the reduction in the probability for the dipole to survive in its original state. Notice that color transparency requires $\hat{S}_{\mathbf{x}\mathbf{x}} = 1$ and thus the potential short-distance singularities, arising from the dipole kernel \mathcal{M} , at $\mathbf{x}_1 = \mathbf{z}$ and $\mathbf{x}_2 = \mathbf{z}$ cancel between the real and virtual terms.

A word of caution should follow here. Eq. (2.12) is valid for any value of N_c , but still, both terms on the right hand side are of the same order in N_c . In fact, terms suppressed by $1/N_c^2$ have been generated in intermediate steps of the calculation but they have canceled in the final result. More precisely, when acting with H_{real} on $\hat{S}_{\mathbf{x}_1 \mathbf{x}_2}$ we get a contribution

$$-\frac{1}{N_c^2} \frac{\bar{\alpha}}{2\pi} \int_{\mathbf{z}} \mathcal{M}_{\mathbf{x}_1 \mathbf{x}_2 \mathbf{z}} \hat{S}_{\mathbf{x}_1 \mathbf{x}_2}, \quad (2.13)$$

which cancels with an opposite in sign contribution coming from the action of H_{virt} .

Similarly one can derive the evolution equation for the quadrupole, which reads

$$\begin{aligned} \frac{\partial \langle \hat{Q}_{\mathbf{x}_1 \mathbf{x}_2 \mathbf{x}_3 \mathbf{x}_4} \rangle_Y}{\partial Y} = & \frac{\bar{\alpha}}{4\pi} \int_{\mathbf{z}} \left[(\mathcal{M}_{\mathbf{x}_1 \mathbf{x}_2 \mathbf{z}} + \mathcal{M}_{\mathbf{x}_1 \mathbf{x}_4 \mathbf{z}} - \mathcal{M}_{\mathbf{x}_2 \mathbf{x}_4 \mathbf{z}}) \langle \hat{S}_{\mathbf{x}_1 \mathbf{z}} \hat{Q}_{\mathbf{z} \mathbf{x}_2 \mathbf{x}_3 \mathbf{x}_4} \rangle_Y \right. \\ & + (\mathcal{M}_{\mathbf{x}_1 \mathbf{x}_2 \mathbf{z}} + \mathcal{M}_{\mathbf{x}_2 \mathbf{x}_3 \mathbf{z}} - \mathcal{M}_{\mathbf{x}_1 \mathbf{x}_3 \mathbf{z}}) \langle \hat{S}_{\mathbf{z} \mathbf{x}_2} \hat{Q}_{\mathbf{x}_1 \mathbf{z} \mathbf{x}_3 \mathbf{x}_4} \rangle_Y \\ & + (\mathcal{M}_{\mathbf{x}_2 \mathbf{x}_3 \mathbf{z}} + \mathcal{M}_{\mathbf{x}_3 \mathbf{x}_4 \mathbf{z}} - \mathcal{M}_{\mathbf{x}_2 \mathbf{x}_4 \mathbf{z}}) \langle \hat{S}_{\mathbf{x}_3 \mathbf{z}} \hat{Q}_{\mathbf{x}_1 \mathbf{x}_2 \mathbf{z} \mathbf{x}_4} \rangle_Y \\ & + (\mathcal{M}_{\mathbf{x}_1 \mathbf{x}_4 \mathbf{z}} + \mathcal{M}_{\mathbf{x}_3 \mathbf{x}_4 \mathbf{z}} - \mathcal{M}_{\mathbf{x}_1 \mathbf{x}_3 \mathbf{z}}) \langle \hat{S}_{\mathbf{z} \mathbf{x}_4} \hat{Q}_{\mathbf{x}_1 \mathbf{x}_2 \mathbf{x}_3 \mathbf{z}} \rangle_Y \\ & - (\mathcal{M}_{\mathbf{x}_1 \mathbf{x}_2 \mathbf{z}} + \mathcal{M}_{\mathbf{x}_3 \mathbf{x}_4 \mathbf{z}} + \mathcal{M}_{\mathbf{x}_1 \mathbf{x}_4 \mathbf{z}} + \mathcal{M}_{\mathbf{x}_2 \mathbf{x}_3 \mathbf{z}}) \langle \hat{Q}_{\mathbf{x}_1 \mathbf{x}_2 \mathbf{x}_3 \mathbf{x}_4} \rangle_Y \\ & - (\mathcal{M}_{\mathbf{x}_1 \mathbf{x}_2 \mathbf{z}} + \mathcal{M}_{\mathbf{x}_3 \mathbf{x}_4 \mathbf{z}} - \mathcal{M}_{\mathbf{x}_1 \mathbf{x}_3 \mathbf{z}} - \mathcal{M}_{\mathbf{x}_2 \mathbf{x}_4 \mathbf{z}}) \langle \hat{S}_{\mathbf{x}_1 \mathbf{x}_2} \hat{S}_{\mathbf{x}_3 \mathbf{x}_4} \rangle_Y \\ & \left. - (\mathcal{M}_{\mathbf{x}_1 \mathbf{x}_4 \mathbf{z}} + \mathcal{M}_{\mathbf{x}_2 \mathbf{x}_3 \mathbf{z}} - \mathcal{M}_{\mathbf{x}_1 \mathbf{x}_3 \mathbf{z}} - \mathcal{M}_{\mathbf{x}_2 \mathbf{x}_4 \mathbf{z}}) \langle \hat{S}_{\mathbf{x}_3 \mathbf{x}_2} \hat{S}_{\mathbf{x}_1 \mathbf{x}_4} \rangle_Y \right]. \quad (2.14) \end{aligned}$$

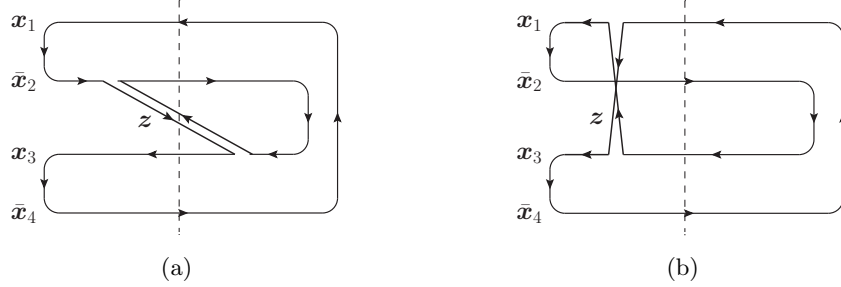


FIG. 3. (a) A real emission of a gluon from a color quadrupole in the large- N_c limit corresponding to the term proportional to $\mathcal{M}_{x_2 x_3 z} \hat{S}_{z x_2} \hat{Q}_{x_1 z x_3 x_4}$. (b) A virtual emission corresponding to the term proportional to $-\mathcal{M}_{x_1 x_3 z} \hat{S}_{x_3 x_2} \hat{S}_{x_1 x_4}$. In both diagrams the dashed line denotes the interaction with the target.

Even though this looks considerably more involved than the dipole equation, a similar discussion applies and two representative diagrams are shown in Fig. 3. The terms involving $\langle \hat{S} \hat{Q} \rangle_Y$ in the right hand side are real terms describing the splitting of the original quadrupole into a new quadrupole plus a dipole, and have generated by the action H_{real} . The virtual terms involving $\langle \hat{Q} \rangle_Y$ and $\langle \hat{S} \hat{S} \rangle_Y$ are necessary for probability conservation, and have been generated by H_{virt} . Once again, all terms subleading at large N_c , separately generated by the two parts of the Hamiltonian, have canceled in the final equation, and all the short-distance singularities of the dipole kernels at $x_i = z$, with $i = 1, 2, 3, 4$, cancel among the various terms.

All the above features generalize to the evolution equations obeyed by the single-trace observables given in Eq. (2.9). As already evident in Eqs. (2.12) and (2.14), these equations are generally not closed and they couple single-trace observables with multi-trace ones. For instance, the quadrupole equation involves the 4-point function $\langle \hat{S} \hat{S} \rangle_Y$ and the 6-point function $\langle \hat{S} \hat{Q} \rangle_Y$, which in turn will couple to even higher-point correlators. The equations obeyed by the multi-trace observables exhibit the new feature that they involve explicit $1/N_c^2$ corrections. These arise when two functional derivatives in Eq. (2.2) act on Wilson lines which belong to different traces (see e.g. Appendix F in [53] for an example). At large N_c , one can neglect these terms and check that the hierarchy admits the factorized solution

$$\langle \hat{\mathcal{O}} \rangle_Y \simeq \left\langle \frac{1}{N_c} \text{tr}(V_{x_1}^\dagger V_{x_2} \dots) \right\rangle_Y \left\langle \frac{1}{N_c} \text{tr}(V_{y_1}^\dagger V_{y_2} \dots) \right\rangle_Y \left\langle \frac{1}{N_c} \text{tr}(V_{z_1}^\dagger V_{z_2} \dots) \right\rangle_Y \dots, \quad (2.15)$$

so long as this factorization is already present in the initial condition. Therefore the hierarchy simplifies in a drastic way as it decomposes into a set of equations which can be solved, in principle, one after the other. More precisely, Eq. (2.12) becomes a closed equation for $\langle \hat{S} \rangle_Y$, the well-known BK equation [48, 49], Eq. (2.14) becomes an inhomogeneous equation for $\langle \hat{Q} \rangle_Y$ whose coefficients depend on $\langle \hat{S} \rangle_Y$ [17], and so on. Good analytical understanding and reliable numerical solutions to the BK equation exist, and we will discuss these matters in the next section. However, already starting from the quadrupole, it seems difficult to numerically deal with the large number of variables in the higher-point equations and the non-locality in the transverse space at the same time. In that case one can rely on an alternative formulation of the JIMWLK evolution as a Langevin equation [39] which can be solved on a lattice [40, 54, 55], or develop well-motivated approximate schemes and we shall turn our attention to the latter in Sect. IV.

III. SOLUTION TO THE BK EQUATION AND THE LEVIN-TUCHIN FORMULA

Let us briefly review the analytic solution to the BK equation. We shall assume a homogeneous target so that the amplitude $\langle \hat{T}_{\mathbf{x}_1 \mathbf{x}_2} \rangle_Y = 1 - \langle \hat{S}_{\mathbf{x}_1 \mathbf{x}_2} \rangle_Y$ depends only on the magnitude $r \equiv r_{12} = |\mathbf{x}_1 - \mathbf{x}_2|$. Still, the solution is not analytically known, but one can construct a piecewise one when $\bar{\alpha}Y \gtrsim 1$, by considering two regimes. The regime $r \lesssim 1/Q_s$ where the target is dilute and the scattering weak and the regime $r \gtrsim 1/Q_s$ where the target is dense and the scattering strong. The borderline in between corresponds to the saturation momentum Q_s and can be determined from the solution to the BFKL equation, that is, the linearized in \hat{T} version of the BK equation, supplemented by appropriate boundary conditions. For fixed coupling one finds that the energy dependence of the saturation momentum is determined by [56, 57]

$$\frac{1}{\bar{\alpha}} \frac{d \ln Q_s^2}{dY} = \frac{\chi(\gamma_s)}{\gamma_s} - \frac{3}{2\gamma_s} \frac{1}{\bar{\alpha}Y}, \quad (3.1)$$

where the “anomalous dimension” γ_s related to saturation is determined by [58]

$$\chi'(\gamma_s) = \chi(\gamma_s)/\gamma_s \Rightarrow \gamma_s \approx 0.628. \quad (3.2)$$

In the above, $\chi(\gamma)$ is the eigenvalue function of the BFKL equation [59, 60] given by

$$\chi(\gamma) = 2\psi(1) - \psi(\gamma) - \psi(1 - \gamma), \quad (3.3)$$

with ψ the logarithmic derivative of the Γ -function. The amplitude on this side of the saturation line, that is for $r \ll 1/Q_s$, reads [56, 57]

$$\langle \hat{T} \rangle_Y = (r^2 Q_s^2)^{\gamma_s} \ln \left(\frac{1}{r^2 Q_s^2} + c \right) \exp \left[-\frac{\ln^2(r^2 Q_s^2)}{D_s \bar{\alpha}Y} \right], \quad (3.4)$$

an expression which is valid in the region $Q_s^2 \ll 1/r^2 \ll Q_s^2 \exp(D_s \bar{\alpha}Y)$, where c is a constant of order $\mathcal{O}(1)$ and $D_s = 2\chi''(\gamma_s) \approx 97$ is the diffusion coefficient. When $|\ln(r^2 Q_s^2)| \ll \sqrt{D_s \bar{\alpha}Y}$ the last factor in Eq. (3.4), which describes diffusion, can be set equal to unity and the amplitude exhibits geometrical scaling [56, 57, 61–63]; it depends only on the combined variable $r^2 Q_s^2$.

Let us now look at what happens when $r \gg 1/Q_s$. In this regime the S -matrix approaches its black-disk limit, i.e. $\langle \hat{S} \rangle_Y \rightarrow 0$, and thus we can neglect the term quadratic in $\langle \hat{S} \rangle_Y$ in the BK equation. To do this properly, we need to restrict the region of integration in the transverse coordinates to $1/Q_s^2 \ll |\mathbf{x}_i - \mathbf{z}|^2 \ll r^2$, with $i = 1, 2$. The lower limit emerges as the boundary determining the transition from a region where the scattering is weak to a region where it becomes strong. The upper limit determines the dominant logarithmic contribution to the r.h.s. of the BK equation. We easily find that

$$\frac{\partial \langle \hat{S} \rangle_Y}{\partial Y} = -\bar{\alpha} \int_{1/Q_s^2}^{r^2} \frac{dz^2}{z^2} \langle \hat{S} \rangle_Y = -\bar{\alpha} \ln(r^2 Q_s^2) \langle \hat{S} \rangle_Y, \quad (3.5)$$

and using the leading behavior for the rapidity dependence of Q_s given in Eq. (3.1) we convert the derivative w.r.t. Y to one w.r.t. $\ln(r^2 Q_s^2)$. Then it becomes trivial to solve Eq. (3.5) and we arrive at

$$\langle \hat{S} \rangle_Y \sim \exp \left[-\frac{\gamma_s}{2\chi(\gamma_s)} \ln^2(r^2 Q_s^2) \right], \quad (3.6)$$

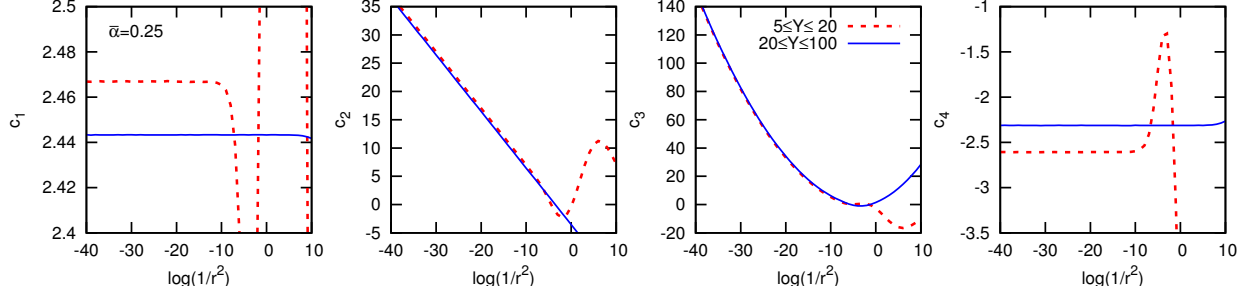


FIG. 4. Numerical extraction of the coefficients in the asymptotic expansion (3.9) at saturation and for fixed coupling. The coefficients are plotted as a function of the dipole size r .

where it should be reminded that only this leading term in the exponent is under good control. Eq. (3.6) is equivalent in its functional form to the Levin-Tuchin formula [43] (see also [44–47]), apart from the coefficient in the exponent which is different. Let us also add here, that this coefficient is further modified when N_c is finite, namely the exponent should be multiplied by a factor $2C_F/N_c = (N_c^2 - 1)/N_c^2$ [42, 46]. Again, geometric scaling is manifest in Eq. (3.6) and in fact this property is valid everywhere in the region $\Lambda_{\text{QCD}}^2 \ll 1/r^2 \ll Q_s^2 \exp[\sqrt{D_s \bar{\alpha} Y}]$. Even though we do not have an analytical solution to cover the whole region, one can construct appropriate interpolations. For instance, and neglecting also the second factor in Eq. (3.4) which has only a weak logarithmic dependence, such a convenient expression is

$$\langle \hat{S} \rangle_Y = \exp \left\{ -\frac{2}{\gamma_s \chi(\gamma_s)} \ln^2 [1 + b(rQ_s)^{\gamma_s}] \right\}, \quad (3.7)$$

with b a constant of order $\mathcal{O}(1)$.

Going back to Eq. (3.6) and using Eq. (3.1), let us note that, for fixed r , the dominant term in the exponent is proportional to the square of Y . This has a direct physical interpretation which should have been obvious from the derivation. One factor of Y already appears in zero-dimensional particle models where all transverse coordinates are suppressed and represents the fact that dP/dY is proportional to $-P$, where P is the probability that a particle does not split. An extra factor of Y arises in QCD because the available phase space for an emission of a gluon increases with $\ln(Q_s^2) \sim Y$.

Here we shall put forward the task to numerically verify Eq. (3.6) for two reasons. The first is simply that such a study has not been done so far (see [44] for a related work). The second is that it is necessary for the comparisons to be performed in Sect. V. To this end, by also using Eq. (3.1), we can write the large- Y and large- $\ln(1/r^2)$ expansion

$$-\ln \langle \hat{S} \rangle_Y = \frac{\chi(\gamma_s)}{2\gamma_s} (\bar{\alpha} Y)^2 - \ln \frac{1}{r^2} (\bar{\alpha} Y) + \frac{\gamma_s}{2\chi(\gamma_s)} \ln^2 \frac{1}{r^2} - \frac{3}{2\gamma_s} (\bar{\alpha} Y) \ln(\bar{\alpha} Y). \quad (3.8)$$

We compare this expression with fits of the rapidity dependence of numerical solutions of the BK equation² with a function of the form

$$-\ln \langle \hat{S} \rangle_Y = c_1 (\bar{\alpha} Y)^2 + c_2 (\bar{\alpha} Y) + c_3 + c_4 (\bar{\alpha} Y) \ln(\bar{\alpha} Y). \quad (3.9)$$

² Details about the numerical implementation of the BK equation and the other evolution equations considered later in this article are given in appendix.

Coefficient	c_1	$c_2/\ln(1/r^2)$	$c_3/\ln^2(1/r^2)$	c_4
Analytical	$\chi(\gamma_s)/2\gamma_s = 2.442$	-1	$\gamma_s/2\chi(\gamma_s) = 0.1024$	$-3/2\gamma_s = -2.390$
Numerical ($5 < Y < 20$)	2.466	-1.002	0.1029	-2.601
Numerical ($20 < Y < 200$)	2.443	-1.000	0.1045	-2.313

TABLE I. Analytical and numerical values of the coefficients in the asymptotic expansion of $-\ln\langle\hat{S}(r)\rangle_Y$ at saturation as in Fig. 4. The agreement of the numerics in Fig. 4 with Eq. (3.8) is excellent.

The excellent numerical verification of all terms in (3.8) is demonstrated in Fig. 4 and in Table I. This makes clear that Eq. (3.6), including the exact coefficient in the exponent, gives the correct approach to the unitarity limit within the context of the BK equation. Notice that the asymptotics sets quite fast and the Levin-Tuchin law is valid also for “reasonable” values of Y , albeit this happens for rather large dipoles. Furthermore, it is remarkable that, without focusing in the transition region around Q_s , we get a numerical confirmation for the first two terms of its energy dependence as given in Eq. (3.1).

It is not hard to see how the above description is modified when we consider the running coupling BK equation [64–66]. In general, the coupling runs according to

$$\bar{\alpha}(r) = \frac{1}{\bar{b} \ln(1/r^2 \Lambda_{\text{QCD}}^2)} \quad \text{with} \quad \bar{b} = \frac{11N_c - 2N_f}{12N_c}, \quad (3.10)$$

and where one would need an appropriate prescription to freeze it when r starts to approach $1/\Lambda_{\text{QCD}}$. Now the energy dependence of the saturation momentum reads [56, 57, 67, 68]

$$\frac{d \ln Q_s^2}{dY} = \sqrt{\frac{\chi(\gamma_s)}{2\bar{b}\gamma_s}} \frac{1}{Y} - \frac{|\xi_1|}{8} \left[\frac{\chi''(\gamma_s)}{\chi(\gamma_s)} \right]^{1/3} \left[\frac{\chi(\gamma_s)}{2\bar{b}\gamma_s} \right]^{1/6} \frac{1}{Y^{5/6}}, \quad (3.11)$$

with $\xi_1 = -2.33$ the leftmost zero of the Airy function. In order to find the behavior of the S -matrix at saturation, we make in Eq. (3.5) the replacement

$$\bar{\alpha} \rightarrow \frac{1}{\bar{b} \ln(1/z^2 \Lambda_{\text{QCD}}^2)}, \quad (3.12)$$

and where clearly this factor has to be moved inside the integrand. Notice that such a replacement can be obtained from a “smallest dipole” prescription, which is a natural one³; given the dipole splitting $(\mathbf{x}_1, \mathbf{x}_2) \rightarrow (\mathbf{x}_1, \mathbf{z})$ and $(\mathbf{z}, \mathbf{x}_2)$ we let the coupling run according to $\bar{\alpha}(r_{\min})$, with r_{\min} the size of the smallest of the three dipoles involved in the process. We find [46]

$$\frac{\partial \langle \hat{S} \rangle_Y}{\partial Y} = -\frac{1}{\bar{b}} \ln \left[\frac{\ln(Q_s^2/\Lambda_{\text{QCD}}^2)}{\ln(1/r^2 \Lambda_{\text{QCD}}^2)} \right] \langle \hat{S} \rangle_Y, \quad (3.13)$$

and after the integration by keeping only the most dominant term in Y we obtain

$$\langle \hat{S} \rangle_Y \sim \exp \left(-\frac{1}{2\bar{b}} Y \ln Y \right). \quad (3.14)$$

³ In the subsequent sections we shall extend our study to include two more prescriptions: the Balitsky prescription [65] which has dominated the phenomenology in the recent years, and a particular daughter dipole prescription which is used when one solves the Langevin form of the JIMWLK equation [40, 55].

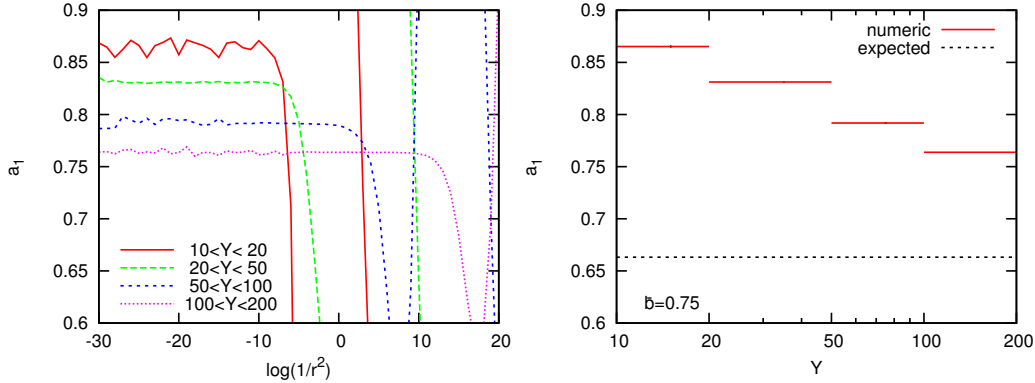


FIG. 5. Numerical extraction of the coefficient a_1 in the asymptotic expansion $-\ln\langle\hat{S}(r)\rangle_Y = a_1 Y \ln Y + a_2 Y + a_3 \ln Y + a_4$ at saturation and for running coupling.

In the numerical solution shown in Fig. 5 we see that one indeed recovers this dependence in Y without the need to evolve too much. However the value of the coefficient differs around 30% from its asymptotic value $1/2\bar{b}$. The approach to the latter is extremely slow and takes place only at tremendously high values of Y .

IV. THE GAUSSIAN APPROXIMATION

As said at the end of Sect. II, one method to calculate multi-gluon correlators is to solve the Langevin form of the JIMWLK equation on a lattice [39]. The implementation of this approach [40] lead to the remarkable finding that the numerical data for the quadrupole are well-described by a Gaussian approximation, more precisely by the extension of the MV model to arbitrary rapidity Y . We shall not review here the MV model, but it suffices for our purposes to recall that it is the typical initial condition at some Y_0 . It is a Gaussian functional in the color sources ρ_a and therefore also in the field α_a in the covariant gauge, but with a kernel which is independent of Y , since it refers to a fixed, initial, value of rapidity. Furthermore, it is clear that any Gaussian probability distribution involves only a single kernel, thus all high-point correlators can be expressed in terms of the 2-point one, e.g. the dipole S -matrix $\langle\hat{S}\rangle_Y$, a property which is true in the MV-model. Nevertheless, there was no a priori reason for this to happen for the JIMWLK Hamiltonian which is highly non-linear due to the Wilson lines in Eq. (2.2) and which arise, as said, from the scattering of the emitted gluon with the existing background target field. Perhaps a hint was given some time ago in [69], where a “random phase approximation” to JIMWLK lead to a Gaussian Hamiltonian, even though no explicit reference to high-point correlators was made there. A Gaussian ansatz has also been used in [70] in order to estimate $1/N_c^2$ corrections to the BK equation.

Still, despite the aforementioned nonlinearities, one can prove that a Gaussian approximation is a quasi-exact solution to the JIMWLK equation [41, 42]. The non-linearity is indeed present in the dipole equation given in Eq. (2.12), but not in the quadrupole one, Eq. (2.14), which is linear in \hat{Q} (at the operator level and/or at large- N_c). This is an indication that a Gaussian approximation

may be a possible solution with all the non-linearities absorbed in its kernel or, equivalently, in the 2-point function. Let us shortly review and explain how this happens [41, 42].

At saturation, where by definition the target is dense, real emissions are suppressed and the virtual part H_{virt} of the Hamiltonian dominates. This part has obviously a Gaussian form, including the second term; those adjoint Wilson lines simply transform the “left” functional derivatives to “right” ones which act on the lower and upper end-points of the Wilson lines V^\dagger and V respectively, namely

$$(\tilde{V}_u^\dagger)^{ac} \frac{\delta}{\delta \alpha_u^a} V_x^\dagger = (\tilde{V}_u^\dagger)^{cb} \frac{\delta}{\delta \alpha_u^b} V_x^\dagger \equiv \frac{\delta}{\delta \alpha_{Ru}^a} V_x^\dagger = ig \delta_{xu} V_x^\dagger t^c, \quad (4.1)$$

and similarly for the action on V_x .

Now we proceed as in the case of the BK equation. Since the integrand of H_{virt} is z -independent, we can integrate the dipole kernel over z in the region $1/Q_s^2 \ll |\mathbf{u} - \mathbf{z}|^2, |\mathbf{v} - \mathbf{z}|^2 \ll |\mathbf{u} - \mathbf{v}|^2$. Again the lower limit is imposed by our approximation, while the upper one is chosen to give the dominant logarithmic contribution which is $2 \ln [(\mathbf{u} - \mathbf{v})^2 Q_s^2]$. So far our approach would lead to a Hamiltonian valid only at saturation, but recalling Eq. (3.5) we see that this logarithm can be expressed in terms of the logarithmic derivative of the dipole w.r.t. Y and with such a replacement we finally arrive at

$$H_G = \frac{1}{4g^2 C_F} \int_{uv} \frac{d \ln \langle \hat{S}_{uv} \rangle_Y}{dY} \left(\frac{\delta}{\delta \alpha_{Lu}^a} \frac{\delta}{\delta \alpha_{Lv}^a} + \frac{\delta}{\delta \alpha_{Ru}^a} \frac{\delta}{\delta \alpha_{Rv}^a} \right). \quad (4.2)$$

This is a Gaussian Hamiltonian which is correct, for finite- N_c , at saturation by construction and in the dilute limit as can be inspected. The kernel, which has absorbed the non-linearities, is Y -dependent (in contrast to the MV model one) and is most easily determined from the BK equation. Indeed one can verify that in the Gaussian approximation, and in an arbitrary representation R , we have

$$\ln \langle \hat{S}_{uv}^R \rangle_Y = \frac{2C_R}{N_c} \ln \langle \hat{S}_{uv}^{\text{BK}} \rangle_Y, \quad (4.3)$$

and insert it for $R = F$ in Eq. (4.2). Therefore, by solving the BK equation, a closed equation at large- N_c , we can first find the dipole S -matrix at finite- N_c using Eq. (4.3). Then, using H_G one constructs evolution equations for high-point correlators which have the advantage to be local in the transverse plane, which simply means they are ordinary differential equations in Y with Y -dependent coefficients. For example, the quadrupole at large- N_c , on which we will focus in Sect. VI, reads [41, 42]

$$\begin{aligned} \langle \hat{Q}_{\mathbf{x}_1 \mathbf{x}_2 \mathbf{x}_3 \mathbf{x}_4} \rangle_Y &= \sqrt{\langle \hat{S}_{\mathbf{x}_1 \mathbf{x}_2} \rangle_Y \langle \hat{S}_{\mathbf{x}_3 \mathbf{x}_2} \rangle_Y \langle \hat{S}_{\mathbf{x}_3 \mathbf{x}_4} \rangle_Y \langle \hat{S}_{\mathbf{x}_1 \mathbf{x}_4} \rangle_Y} \left[\frac{\langle \hat{Q}_{\mathbf{x}_1 \mathbf{x}_2 \mathbf{x}_3 \mathbf{x}_4} \rangle_{Y_0}}{\sqrt{\langle \hat{S}_{\mathbf{x}_1 \mathbf{x}_2} \rangle_{Y_0} \langle \hat{S}_{\mathbf{x}_3 \mathbf{x}_2} \rangle_{Y_0} \langle \hat{S}_{\mathbf{x}_3 \mathbf{x}_4} \rangle_{Y_0} \langle \hat{S}_{\mathbf{x}_1 \mathbf{x}_4} \rangle_{Y_0}}} \right. \\ &\quad \left. + \frac{1}{2} \int_{Y_0}^Y dy \frac{\langle \hat{S}_{\mathbf{x}_1 \mathbf{x}_3} \rangle_y \langle \hat{S}_{\mathbf{x}_2 \mathbf{x}_4} \rangle_y}{\sqrt{\langle \hat{S}_{\mathbf{x}_1 \mathbf{x}_2} \rangle_y \langle \hat{S}_{\mathbf{x}_3 \mathbf{x}_2} \rangle_y \langle \hat{S}_{\mathbf{x}_3 \mathbf{x}_4} \rangle_y \langle \hat{S}_{\mathbf{x}_1 \mathbf{x}_4} \rangle_y}} \frac{\partial}{\partial y} \frac{\langle \hat{S}_{\mathbf{x}_1 \mathbf{x}_2} \rangle_y \langle \hat{S}_{\mathbf{x}_3 \mathbf{x}_4} \rangle_y + \langle \hat{S}_{\mathbf{x}_1 \mathbf{x}_4} \rangle_y \langle \hat{S}_{\mathbf{x}_3 \mathbf{x}_2} \rangle_y}{\langle \hat{S}_{\mathbf{x}_1 \mathbf{x}_3} \rangle_y \langle \hat{S}_{\mathbf{x}_2 \mathbf{x}_4} \rangle_y} \right]. \quad (4.4) \end{aligned}$$

The quadrupole above obeys the “mirror symmetry” $\langle \hat{Q}_{\mathbf{x}_1 \mathbf{x}_2 \mathbf{x}_3 \mathbf{x}_4} \rangle_Y = \langle \hat{Q}_{\mathbf{x}_1 \mathbf{x}_4 \mathbf{x}_3 \mathbf{x}_2} \rangle_Y$, a property which in fact holds at finite- N_c and beyond the Gaussian approximation and is a consequence of

symmetry under time-reversal where time is represented by x^- [42]. This symmetry is preserved by the JIMWLK equation due to the two types, left and right, of functional derivatives and suggests that the hadron expands symmetrically in the x^- direction during the evolution. At the level of the Gaussian approximation only, the quadrupole is also symmetric under the charge conjugation $\langle \hat{Q}_{\mathbf{x}_1\mathbf{x}_2\mathbf{x}_3\mathbf{x}_4} \rangle_Y = \langle \hat{Q}_{\mathbf{x}_2\mathbf{x}_3\mathbf{x}_4\mathbf{x}_1} \rangle_Y$. It is also important to check the weak scattering limit of Eq. (4.4); when all $\langle \hat{T}_{\mathbf{x}_i\mathbf{x}_j} \rangle_Y = 1 - \langle \hat{S}_{\mathbf{x}_i\mathbf{x}_j} \rangle_Y$ are small, then the expansion of Eq. (4.4) to first order in $\langle \hat{T} \rangle_Y$ reads

$$\langle \hat{Q}_{\mathbf{x}_1\mathbf{x}_2\mathbf{x}_3\mathbf{x}_4} \rangle_Y = 1 - \langle \hat{T}_{\mathbf{x}_1\mathbf{x}_2} \rangle_Y + \langle \hat{T}_{\mathbf{x}_1\mathbf{x}_3} \rangle_Y - \langle \hat{T}_{\mathbf{x}_1\mathbf{x}_4} \rangle_Y - \langle \hat{T}_{\mathbf{x}_2\mathbf{x}_3} \rangle_Y + \langle \hat{T}_{\mathbf{x}_2\mathbf{x}_4} \rangle_Y - \langle \hat{T}_{\mathbf{x}_3\mathbf{x}_4} \rangle_Y, \quad (4.5)$$

which is assuredly the same relation one finds by expanding the Wilson lines of the dipole and the quadrupole to order $(g\alpha)^2$. Let us also point out that a general initial condition where $\langle \hat{Q} \rangle_{Y_0}$ is not determined by $\langle \hat{S} \rangle_{Y_0}$ like, for example, the one in [71], can be accommodated for the quadrupole in Eq. (4.4).

In some scenarios one can perform analytically the y -integration in an equation like Eq. (4.4) and therefore arrive at a functional expression for a high-point correlator in terms of the dipole which is local in Y . Such a situation is realized for all the simple configurations studied in [40–42] and independently of whether the coupling is running or not. Furthermore, using a “separability” property of the Gaussian kernel [41, 42] in Eq. (4.2) one can show that this is also the case in fixed coupling evolution for an arbitrary configuration. For example, the quadrupole in Eq. (4.4) assuming MV model initial conditions at Y_0 reads

$$\begin{aligned} \langle \hat{Q}_{\mathbf{x}_1\mathbf{x}_2\mathbf{x}_3\mathbf{x}_4} \rangle_Y &= \frac{\ln [\langle \hat{S}_{\mathbf{x}_1\mathbf{x}_2} \rangle_Y \langle \hat{S}_{\mathbf{x}_3\mathbf{x}_4} \rangle_Y / \langle \hat{S}_{\mathbf{x}_1\mathbf{x}_3} \rangle_Y \langle \hat{S}_{\mathbf{x}_2\mathbf{x}_4} \rangle_Y]}{\ln [\langle \hat{S}_{\mathbf{x}_1\mathbf{x}_2} \rangle_Y \langle \hat{S}_{\mathbf{x}_3\mathbf{x}_4} \rangle_Y / \langle \hat{S}_{\mathbf{x}_1\mathbf{x}_4} \rangle_Y \langle \hat{S}_{\mathbf{x}_2\mathbf{x}_3} \rangle_Y]} \langle \hat{S}_{\mathbf{x}_1\mathbf{x}_2} \rangle_Y \langle \hat{S}_{\mathbf{x}_3\mathbf{x}_4} \rangle_Y \\ &+ \frac{\ln [\langle \hat{S}_{\mathbf{x}_1\mathbf{x}_4} \rangle_Y \langle \hat{S}_{\mathbf{x}_2\mathbf{x}_3} \rangle_Y / \langle \hat{S}_{\mathbf{x}_1\mathbf{x}_3} \rangle_Y \langle \hat{S}_{\mathbf{x}_2\mathbf{x}_4} \rangle_Y]}{\ln [\langle \hat{S}_{\mathbf{x}_1\mathbf{x}_4} \rangle_Y \langle \hat{S}_{\mathbf{x}_2\mathbf{x}_3} \rangle_Y / \langle \hat{S}_{\mathbf{x}_1\mathbf{x}_2} \rangle_Y \langle \hat{S}_{\mathbf{x}_3\mathbf{x}_4} \rangle_Y]} \langle \hat{S}_{\mathbf{x}_1\mathbf{x}_4} \rangle_Y \langle \hat{S}_{\mathbf{x}_2\mathbf{x}_3} \rangle_Y. \end{aligned} \quad (4.6)$$

At the formal level this expression was first derived in the MV model [17] at large- N_c and later on generalized at finite- N_c [33]. One non-trivial achievement in [41, 42] was to show when and why it remains (approximately) valid after quantum evolution has been taken into account. Like Eq. (4.4) it also reduces to Eq. (4.5) in the weak scattering limit. We note that for an arbitrary configuration in running coupling evolution one is supposed to use Eq. (4.4), since the arguments leading to Eq. (4.6) do not go through (except in the case that the scale of the running coupling is taken to be Q_s). Still we shall see that, so long as rQ_s is not becoming too large, one can also use the simpler version Eq. (4.6) for practical purposes.

At finite- N_c there is operator mixing and the analogue of Eq. (4.6) involves the diagonalization of a matrix. For example, the quadrupole mixes with the two dipoles operator, while the phenomenologically interesting 6-point operator $\hat{Q}_{\mathbf{x}_1\mathbf{x}_2\mathbf{x}_3\mathbf{x}_4}\hat{S}_{\mathbf{x}_4\mathbf{x}_1}$, appearing in the quark-gluon double inclusive cross section, mixes with two more operators and one can show that the emerging cubic equation has a unique real solution. It goes without saying, analytic expressions for high-point correlators are invaluable in order to reduce the numerical cost for Fourier transforming to momentum space and obtain the desired cross sections.

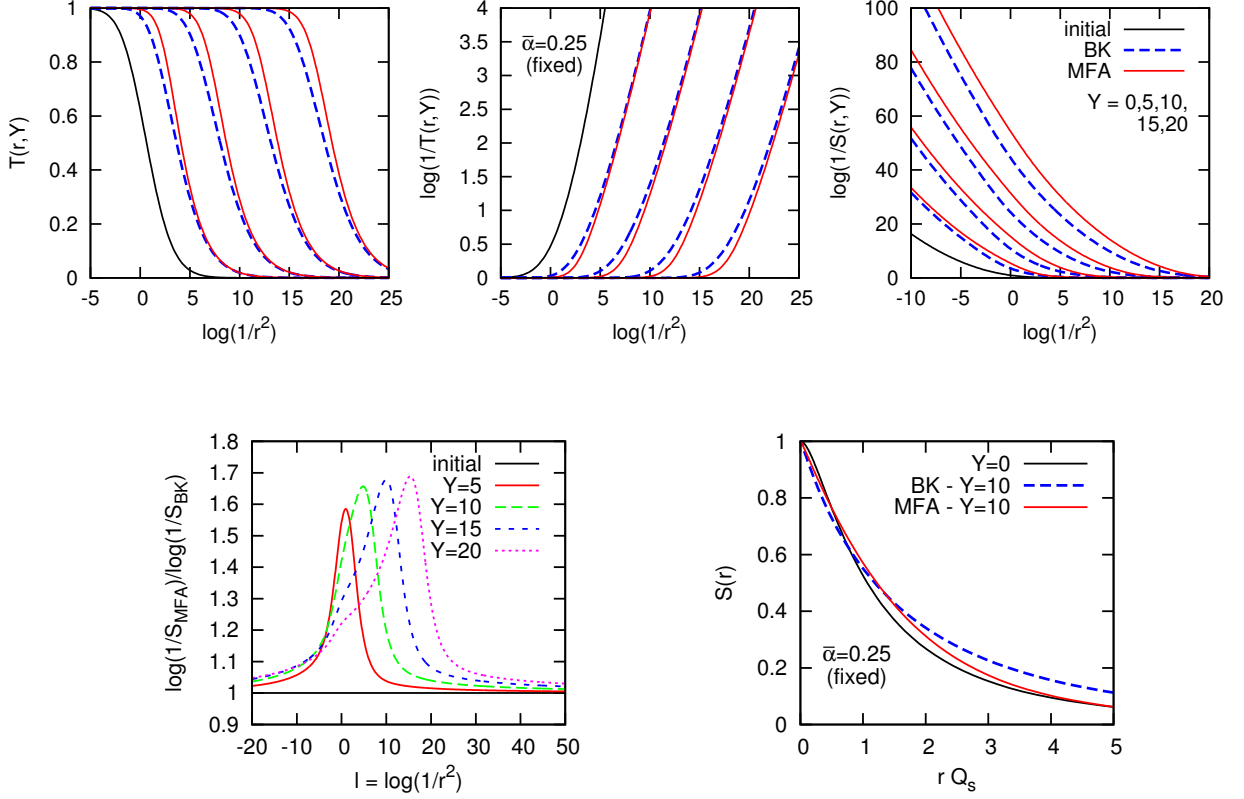


FIG. 6. Precise solution to the BK and MFA equations for fixed coupling.

V. A MEAN FIELD EQUATION

One way to test the accuracy of the approximation scheme is by requiring that the Gaussian Hamiltonian H_G in Eq. (4.2) coincides with the “averaged” JIMWLK Hamiltonian H in Eq. (2.2) [23, 42]. Then it is an easy and straightforward exercise to obtain a *closed* non-linear equation for the dipole in the adjoint representation A which reads [42]

$$\frac{\partial \langle \hat{S}_{\mathbf{x}_1 \mathbf{x}_2}^A \rangle_Y}{\partial Y} = \frac{\bar{\alpha}}{\pi} \int_{\mathbf{z}} \mathcal{M}_{\mathbf{x}_1 \mathbf{x}_2 \mathbf{z}} \frac{\langle \hat{S}_{\mathbf{x}_1 \mathbf{x}_2}^A \rangle_Y}{\langle 1 + \hat{S}_{\mathbf{x}_1 \mathbf{x}_2}^A \rangle_Y} \langle \hat{S}_{\mathbf{x}_1 \mathbf{z}}^A + \hat{S}_{\mathbf{z} \mathbf{x}_2}^A - \hat{S}_{\mathbf{x}_1 \mathbf{x}_2}^A - 1 \rangle_Y. \quad (5.1)$$

We shall study the solution to the above in the large- N_c limit, in which $\langle \hat{S}_{\mathbf{x}_1 \mathbf{x}_2}^A \rangle_Y = \langle \hat{S}_{\mathbf{x}_1 \mathbf{x}_2}^2 \rangle_Y$ and then compare to that of the BK equation. A quick inspection shows that Eq. (5.1) reduces to the BFKL equation in the limit of weak scattering and to Eq. (3.5), like the BK equation, in the regime of strong scattering.

This expected analytic behavior is in fact observed when we compare the numerical simulations of the BK equation Eq. (2.12) to the simulations of the MFA equation (5.1). In Fig. 6 we do see that the two equations, using the same initial condition, agree in the regime of weak scattering. When approaching the saturation regime the two solutions start to separate and, even though $\langle \hat{S} \rangle_Y^{\text{BK}}$ and $\langle \hat{S} \rangle_Y^{\text{MFA}}$ are not the same at saturation, their logarithms agree quite well as we can easily infer from the right plot in the upper panel and the left plot in the lower panel of Fig. 6 and

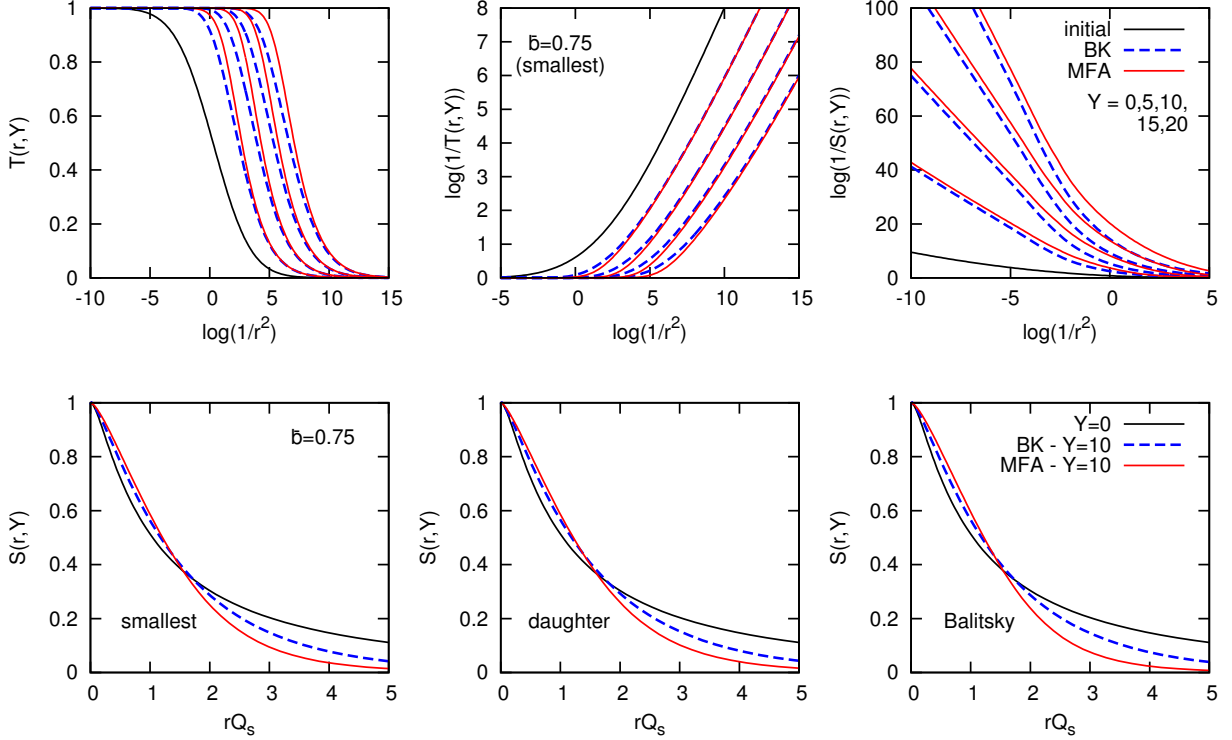


FIG. 7. Precise solution to the BK and MFA equations for running coupling. Above: smallest dipole prescription. Below: Linear scale plots for various schemes for the running of the coupling.

as was advocated at the beginning.

Eq. (5.1) is equally good in running coupling evolution so long as we adopt, as we should, the same prescription for the running of the coupling in both the BK and JIMWLK equations and indeed this is what is shown in Fig. 7. In the upper panel we show the results for the smallest dipole prescription, introduced earlier in Sect. III, which are similar to the fixed coupling ones in the upper panel of Fig. Eq. (6). Even though not shown in a logarithmic scale, to avoid a proliferation of plots, the results for the daughter dipole prescription as in [40, 55] and the Balitsky prescription as in [65], are almost identical in shape⁴. In fact this property can be inferred from the linear plots in the lower panel of Fig. 7.

We shall see in the next Section that, when we express higher-point correlators in terms of the dipole, the accuracy is not restricted to the logarithmic level.

VI. QUADRUPOLE CONFIGURATIONS

Ideally, one would like to solve the quadrupole equation in general. In principle this is possible since it is a closed equation (at large- N_c), but one understands that in practice it is rather com-

⁴ Here we mention the observation of a “peculiar”, and perhaps unphysical, feature already pointed out in [72]: the solutions (for both BK and MFA) with the Balitsky prescription evolve slower than those with the smallest dipole one. In [65, 66] it was shown that the Balitsky prescription is equivalent to the smallest dipole one in the limits where the dipoles sizes are very different. However one can see that when the daughter dipoles are large, that is when $|\mathbf{x}_1 - \mathbf{z}| \simeq |\mathbf{x}_2 - \mathbf{z}| \gg |\mathbf{x}_1 - \mathbf{x}_2|$ then one finds $\bar{\alpha}_{\text{Bal}} \simeq \bar{\alpha}(|\mathbf{x}_1 - \mathbf{x}_2|)(1 - 4\bar{\alpha}(|\mathbf{x}_1 - \mathbf{z}|))$ and therefore this convergence is very slow.

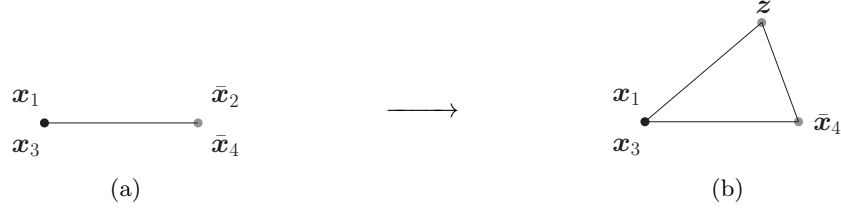


FIG. 8. (a) The “line” configuration of the quadrupole for which $r_{12} = r_{14} = r_{23} = r_{34}$ with $r_{13} = r_{24} = 0$. (b) A triangle configuration emerging from the evolution of the “line”.

plicated, because of the large number of transverse variables (8 in general, 6 if we assume impact-parameter independence and 5 if we also impose rotational invariance) on which the quadrupole depends and because of the non-locality in the transverse plane. Therefore we have to be more modest in our goals, and what we shall do is to average the quadrupole with a Gaussian wavefunction, thus obtaining an evolution equation for the dipole. The solution to the latter will be compared with the solution to the BK equation, and such a comparison should give us a good estimate of the validity of the Gaussian approximation. Still, many coordinates appear in such a general equation and therefore we shall consider only a couple of special configurations. We shall immediately see that the one of them can be analytically investigated.

a. The “line” configuration To start, let us consider the “line” configuration of the quadrupole, as shown in Fig. 8.(a), where we put the two quarks at the same coordinate and similarly for the two antiquarks. This is the simplest possible one, since it is characterized by only one non-vanishing distance, and its evolution, according to Eq. (2.14), is given by

$$\frac{\partial \langle \hat{Q}_{x_1 x_2 x_1 x_2} \rangle_Y}{\partial Y} = \frac{\bar{\alpha}}{\pi} \int_z \mathcal{M}_{x_1 x_2 z} \langle \hat{S}_{x_1 z} \hat{Q}_{z x_2 x_1 x_2} + \hat{S}_{z x_2} \hat{Q}_{x_1 z x_1 x_2} - \hat{Q}_{x_1 x_2 x_1 x_2} - \hat{S}_{x_1 x_2}^2 \rangle_Y. \quad (6.1)$$

Let us assume the large- N_c limit, so that we can factorize $\langle \hat{S} \hat{Q} \rangle_Y \rightarrow \langle \hat{S} \rangle_Y \langle \hat{Q} \rangle_Y$ and $\langle \hat{S}^2 \rangle_Y \rightarrow \langle \hat{S} \rangle_Y^2$. Then the above equation becomes a closed equation for the quadrupole, where the dipole is known from the solution to the BK equation. Still, as expected, this is not a closed equation for the particular quadrupole configuration, since a more general one appears in the real terms on the r.h.s. of the equation. It has the shape of a triangle as shown in Fig. 8.(b); only the two quarks are at the same point with the two antiquarks being separated, or vice versa. As we have said above, we shall assume a Gaussian average over Eq. (6.1), and use (4.6) in order to obtain an equation for the dipole. To this end we need the corresponding average for the configurations appearing in Eq. (6.1) and which are given by or obtained from (always in the large- N_c limit)

$$\langle \hat{Q}_{x_1 z x_1 x_2} \rangle_Y = \langle \hat{S}_{x_1 x_2} \rangle_Y \langle \hat{S}_{x_1 z} \rangle_Y [1 + \ln(\langle \hat{S}_{x_1 x_2} \rangle_Y \langle \hat{S}_{x_1 z} \rangle_Y / \langle \hat{S}_{x_2 z} \rangle_Y)], \quad (6.2)$$

and then Eq. (6.1) leads to

$$\frac{\partial \langle \hat{S}_{x_1 x_2} \rangle_Y}{\partial Y} = \frac{\bar{\alpha}}{2\pi} \int_z \mathcal{M}_{x_1 x_2 z} [\langle \hat{S}_{x_1 z} \rangle_Y \langle \hat{S}_{z x_2} \rangle_Y - \langle \hat{S}_{x_1 x_2} \rangle_Y]. \quad (6.3)$$

which is nothing else than the BK equation. We would also like to stress here, without going through the details of the derivation, that the above is still true even when N_c remains finite; it is

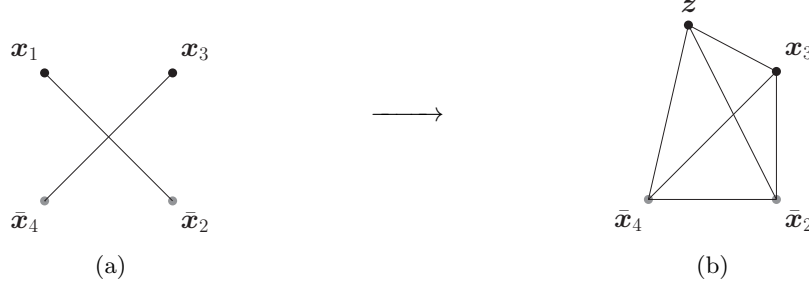


FIG. 9. (a) The “square” configuration of the quadrupole for which $r_{13} = r_{14}$ and $r_{23} = r_{24}$. The average value of \hat{Q} depends only on the distances depicted by straight lines. (b) A configuration emerging from the evolution of the “square”.

a straightforward exercise to show that taking the Gaussian average of Eq. (6.1) we are lead to

$$\frac{\partial \ln \langle \hat{S}_{\mathbf{x}_1 \mathbf{x}_2} \rangle_Y}{\partial Y} = \frac{N_c^2 - 1}{N_c^2} \frac{\bar{\alpha}}{2\pi} \int_{\mathbf{z}} \mathcal{M}_{\mathbf{x}_1 \mathbf{x}_2 \mathbf{z}} \left[\left(\frac{\langle \hat{S}_{\mathbf{x}_1 \mathbf{z}} \rangle_Y \langle \hat{S}_{\mathbf{z} \mathbf{x}_2} \rangle_Y}{\langle \hat{S}_{\mathbf{x}_1 \mathbf{x}_2} \rangle_Y} \right)^{\frac{N_c^2}{N_c^2 - 1}} - 1 \right], \quad (6.4)$$

which is the Gaussian average of the dipole equation at finite- N_c . Moreover, let us note that one arrives again at the above when considering the Gaussian average in the evolution equation of $\langle \hat{S}_{\mathbf{x}_1 \mathbf{x}_2}^2 \rangle_Y$.

All this is a strong indication that the Gaussian approximation should be a very good approximation at least to the particular configurations under consideration. However, one should not draw the conclusion that it is the exact answer. Indeed, one can proceed to assume a Gaussian in the evolution equation of the triangle quadrupole configuration in Fig. 8.(b) to find that this time it does not reduce to the BK equation for the dipole.

b. A “square” configuration Now let us study the configuration shown in 9.(a) where the four fermions are located at the corners of a square⁵. Nevertheless, we prefer to draw the diagonals, for reasons that we immediately explain. Clearly, a “square” configuration is simple enough in the sense that there are only two different distances (the side and the diagonal) between the fermions. This is one of the special class of configurations where the quadrupole can be written as a product of two dipoles in the Gaussian approximation [41, 42]. More precisely, for any value of N_c , one has

$$\langle \hat{Q}_{\mathbf{x}_1 \mathbf{x}_2 \mathbf{x}_3 \mathbf{x}_4} \rangle_Y = \langle \hat{S}_{\mathbf{x}_1 \mathbf{x}_2} \rangle_Y \langle \hat{S}_{\mathbf{x}_3 \mathbf{x}_4} \rangle_Y = \langle \hat{S}(R) \rangle_Y^2, \quad (6.5)$$

where with R we denote the length of the diagonal. The r.h.s. of the quadrupole equation involves quadrupole configurations more complicated than the “square”, e.g. $\langle \hat{Q}_{\mathbf{z} \mathbf{x}_2 \mathbf{x}_3 \mathbf{x}_4} \rangle_Y$, where \mathbf{z} is located anywhere in the 2-dim transverse plane as shown in Fig. 9.(b). This also means that our test of the Gaussian approximation is probing not only the simple square configuration, but also the wider sample of configurations represented by the one in Fig. 9.(b). Using the symmetries of the configuration under consideration we can regroup the terms on the r.h.s. of the equation which

⁵ Notice that this is different than the “square” configuration studied in [40]. There, the two quarks are at the edges of the one diagonal and similarly for the antiquarks. Here, they are at the edges of the same side.

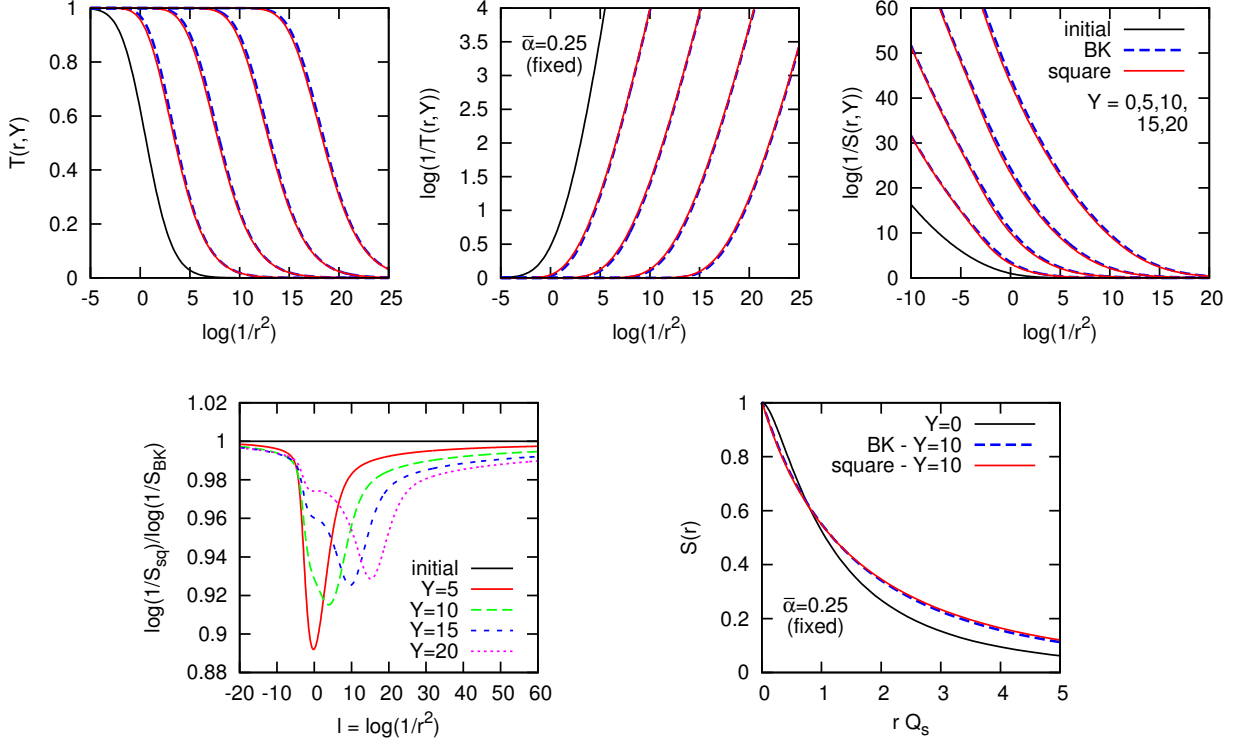


FIG. 10. Solution to the BK and the reduced quadrupole equation for the configuration in Fig. 9 for fixed coupling.

simplifies to

$$\frac{\partial \langle \hat{S}(R) \rangle_Y}{\partial Y} = \frac{\bar{\alpha}}{2\pi} \frac{1}{\langle \hat{S}(R) \rangle_Y} \int_z (\mathcal{M}_{x_1 x_2 z} + \mathcal{M}_{x_1 x_4 z} - \mathcal{M}_{x_2 x_4 z}) [\langle \hat{S}_{x_1 z} \rangle_Y \langle \hat{Q}_{z x_2 x_3 x_4} \rangle_Y - \langle \hat{S}(R) \rangle_Y^2]. \quad (6.6)$$

In general, the quadrupole in the Gaussian approximation and at large- N_c is already given in Eq. (4.4) or its simplified version Eq. (4.6) and we shall use the latter to rewrite (6.6) as a closed equation for $\langle \hat{S}(R) \rangle_Y$. Then considering $\langle \hat{Q}_{z x_2 x_3 x_4} \rangle_Y$ in Eq. (6.6), some minor cancelations occur, since $\langle \hat{S}_{x_2 x_3} \rangle_Y = \langle \hat{S}_{x_2 x_4} \rangle_Y$, but one cannot go far in simplifying the general expression in Eq. (4.6). As a check of our manipulations let us note that in the weak scattering limit Eq. (6.6) reduces to the BFKL equation for $\langle \hat{S}(R) \rangle_Y = \langle \hat{S}_{x_1 x_2} \rangle_Y$, while in the strong scattering regime one recovers to Eq. (3.5). All this is natural if the Gaussian Hamiltonian is expected to be a good approximation scheme.

The numerical results for fixed coupling evolution are shown in Fig. 10 and they should be compared to those of the MFA in Sect. V shown in Fig. 6. It is clear now that the curves arising from the solution to the BK equation and Eq. (6.6) for the square configuration almost fall on top of each other in all kinematic regimes. This is a strong indication that the Gaussian approximation, and more precisely the extrapolation to arbitrary Y of the MV model, is a quasi-exact solution to the JIMWLK equation for fixed coupling evolution.

The situation is almost the same for running coupling evolution and for all the prescriptions used, which are those adopted in Sect. V. This is exhibited in Fig. 11 where one sees that in

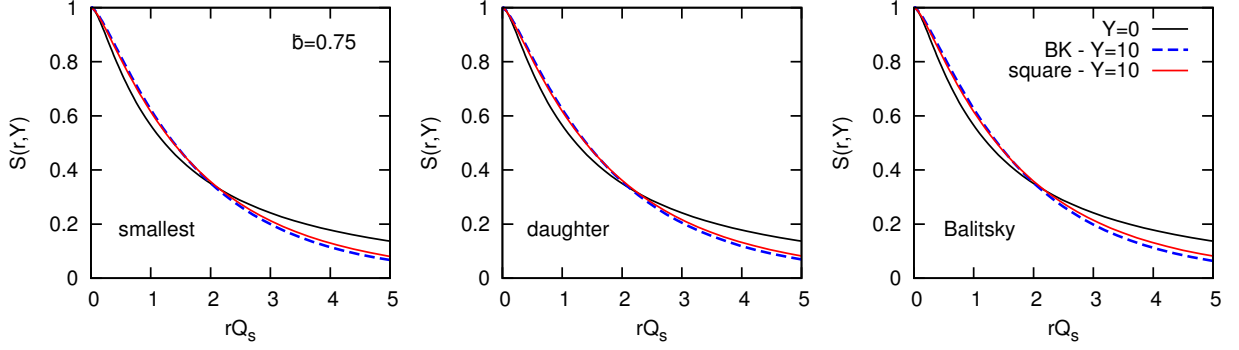


FIG. 11. Solution to the BK and the reduced quadrupole equation for our particular configuration for running coupling.

practice Eq. (4.6) provides an excellent approximation to the quadrupole. Some deviations start to occur when rQ_s becomes large and in fact we have seen in the numerical solutions that these deviations grow and extend deeper in the saturation region when rapidity the Y increases, although an agreement similar to the one observed at fixed coupling is eventually recovered deep in the saturation region. Most likely this discrepancy is to be attributed to the use of Eq. (4.6) instead of the proper expression for running coupling evolution given in Eq. (4.4) (cf. the discussion above and below Eq. (4.6)). This is also supported by the fact that the deviations are stronger (milder) for the Balitsky (daughter dipole) prescription as a consequence of the stronger (milder) variation of the coupling with the scale. Thus, it should be interesting to check if the discrepancy goes away if one makes use of Eq. (4.4), even though this looks to be mostly an academic problem at least for this particular configuration.

VII. CORRELATORS WITH OPEN COLOR INDICES

So far we have dealt with observables which involve only traces over products of Wilson lines. However, there are quantities which require the knowledge of correlators with open color indices, like the energy density and its fluctuations immediately after the collision of two heavy ions, and we shall present here a way to calculate them. We start from the simplest possible case which is the operator $(V_{\mathbf{x}_1}^\dagger V_{\mathbf{x}_2})_{ij}$, with $i, j = 1, 2, \dots, N_c$. Its average value is proportional to the color structure δ_{ij} , so that we must have

$$\langle (V_{\mathbf{x}_1}^\dagger V_{\mathbf{x}_2})_{ij} \rangle_Y = \delta_{ij} \langle \hat{S}_{\mathbf{x}_1 \mathbf{x}_2} \rangle_Y. \quad (7.1)$$

Indeed, if we contract the above with δ_{ij} we arrive at the average of the definition of the dipole $\hat{S}_{\mathbf{x}_1 \mathbf{x}_2}$ as given in Eq. (2.7). This may look rather trivial for the moment but we shall see that the method works for less simple operators with more open color indices. It is also important to point out that the color structure in Eq. (7.1) is preserved under evolution, either JIMWLK or Gaussian. At this level, one needs to be careful and use the more general form of the JIMWLK Hamiltonian

$$H = \frac{1}{8\pi^3} \int_{\mathbf{u} \mathbf{v} \mathbf{z}} \mathcal{K}_{\mathbf{u} \mathbf{v} \mathbf{z}} \frac{\delta}{\delta \alpha_{\mathbf{u}}^a} \left(1 + \tilde{V}_{\mathbf{u}}^\dagger \tilde{V}_{\mathbf{v}} - \tilde{V}_{\mathbf{u}}^\dagger \tilde{V}_{\mathbf{z}} - \tilde{V}_{\mathbf{z}}^\dagger \tilde{V}_{\mathbf{v}} \right)^{ab} \frac{\delta}{\delta \alpha_{\mathbf{v}}^b}, \quad (7.2)$$

with the kernel

$$\mathcal{K}_{\mathbf{uvz}} = \frac{(\mathbf{u} - \mathbf{z}) \cdot (\mathbf{v} - \mathbf{z})}{(\mathbf{u} - \mathbf{z})^2 (\mathbf{v} - \mathbf{z})^2}, \quad (7.3)$$

when acting on Wilson lines with open indices. Considering, as an example, only the last (the one involving $\tilde{V}_z^\dagger \tilde{V}_v$) of the four terms in the parenthesis of Eq. (7.2), it is a straightforward exercise to show that

$$\begin{aligned} \langle H(V_{\mathbf{x}_1}^\dagger V_{\mathbf{x}_2})_{ij} \rangle_Y \Big|_{4\text{th}} &= \frac{\bar{\alpha}}{4\pi} \int_{\mathbf{uvz}} \mathcal{K}_{\mathbf{uvz}} (\delta_{v\mathbf{x}_1} - \delta_{v\mathbf{x}_2}) \left[\delta_{u\mathbf{x}_1} \langle \hat{S}_{\mathbf{x}_1\mathbf{z}} (V_{\mathbf{z}}^\dagger V_{\mathbf{x}_2})_{ij} \rangle_Y - \delta_{u\mathbf{x}_2} \langle (V_{\mathbf{x}_1}^\dagger V_{\mathbf{z}})_{ij} \hat{S}_{\mathbf{z}\mathbf{x}_2} \rangle_Y \right. \\ &\quad \left. - \frac{1}{N_c^2} (\delta_{u\mathbf{x}_1} - \delta_{u\mathbf{x}_2}) \langle (V_{\mathbf{x}_1}^\dagger V_{\mathbf{x}_2})_{ij} \rangle_Y \right]. \end{aligned} \quad (7.4)$$

Now we employ Eq. (7.1) in the last term in the bracket, while we furthermore assume for the first term that

$$\langle \hat{S}_{\mathbf{x}_1\mathbf{z}} (V_{\mathbf{z}}^\dagger V_{\mathbf{x}_2})_{ij} \rangle_Y = \delta_{ij} \langle \hat{S}_{\mathbf{x}_1\mathbf{z}} \hat{S}_{\mathbf{z}\mathbf{x}_2} \rangle_Y, \quad (7.5)$$

and similarly for the second one. Making use of

$$\int_{\mathbf{uv}} \mathcal{K}_{\mathbf{uvz}} (\delta_{u\mathbf{x}_1} - \delta_{u\mathbf{x}_2}) (\delta_{v\mathbf{x}_1} - \delta_{v\mathbf{x}_2}) = \mathcal{M}_{\mathbf{x}_1\mathbf{x}_2\mathbf{z}}, \quad (7.6)$$

we can write

$$\langle H(V_{\mathbf{x}_1}^\dagger V_{\mathbf{x}_2})_{ij} \rangle_Y \Big|_{4\text{th}} = \delta_{ij} \frac{\bar{\alpha}}{4\pi} \int_{\mathbf{z}} \mathcal{M}_{\mathbf{x}_1\mathbf{x}_2\mathbf{z}} \left\langle \hat{S}_{\mathbf{x}_1\mathbf{z}} \hat{S}_{\mathbf{z}\mathbf{x}_2} - \frac{1}{N_c^2} \hat{S}_{\mathbf{x}_1\mathbf{x}_2} \right\rangle_Y = \delta_{ij} \langle H \hat{S}_{\mathbf{x}_1\mathbf{x}_2} \rangle_Y \Big|_{4\text{th}}. \quad (7.7)$$

We can follow the same procedure for all terms of the JIMWLK Hamiltonian to finally arrive at

$$\langle H(V_{\mathbf{x}_1}^\dagger V_{\mathbf{x}_2})_{ij} \rangle_Y = \langle H \delta_{ij} \hat{S}_{\mathbf{x}_1\mathbf{x}_2} \rangle_Y, \quad (7.8)$$

which was our original claim. It means that if Eq. (7.1) and equations of the form (7.5) are valid at rapidity Y , then Eq. (7.1) will hold at $Y + \Delta Y$. Subsequent action of the Hamiltonian will generate operators with more and more Wilson lines, but the only structures that can emerge are $\delta_{ij} \hat{\mathcal{O}}$ (such a term in the above example is not shown in Eq. (7.4) but is generated by the first term of the Hamiltonian) or $(V_{\mathbf{x}_1}^\dagger V_{\mathbf{x}_2} \dots V_{\mathbf{x}_{2n-1}}^\dagger V_{\mathbf{x}_{2n}})_{ij} \hat{\mathcal{O}}$, where $\hat{\mathcal{O}}$ is an operator with no open color indices. This will happen because we are interested in Wilson lines in the fundamental representation; the two functional derivatives of the Hamiltonian give rise to the color structure $(t^a)_{kl} (t^a)_{mn}$ which can be expressed in terms of Kronecker deltas, through the Fierz identity. Thus one finally arrives at the conclusion that (with $\hat{S}^{(2n)}$ given in Eq. (2.9))

$$\langle (V_{\mathbf{x}_1}^\dagger V_{\mathbf{x}_2} \dots V_{\mathbf{x}_{2n-1}}^\dagger V_{\mathbf{x}_{2n}})_{ij} \hat{\mathcal{O}} \rangle_Y = \delta_{ij} \langle \hat{S}_{\mathbf{x}_1\mathbf{x}_2 \dots \mathbf{x}_{2n-1}\mathbf{x}_{2n}}^{(2n)} \hat{\mathcal{O}} \rangle_Y \quad (7.9)$$

will be true for any $\hat{\mathcal{O}}$ with no open color indices and at any value of the rapidity Y , since it is trivially valid for vanishing color gauge field.

Let us now go to a more interesting case by considering the operator $(V_{\mathbf{x}_1}^\dagger V_{\mathbf{x}_2})_{ij} (V_{\mathbf{x}_3}^\dagger V_{\mathbf{x}_4})_{kl} \hat{\mathcal{O}}$. Similar reasoning leads us to expect the color structure

$$\langle (V_{\mathbf{x}_1}^\dagger V_{\mathbf{x}_2})_{ij} (V_{\mathbf{x}_3}^\dagger V_{\mathbf{x}_4})_{kl} \hat{\mathcal{O}} \rangle_Y = \delta_{ij} \delta_{kl} \langle \hat{A} \rangle_Y + \delta_{il} \delta_{jk} \langle \hat{B} \rangle_Y + \delta_{ik} \delta_{jl} \langle \hat{C} \rangle_Y, \quad (7.10)$$

and by contracting with $\delta_{ij}\delta_{kl}$, $\delta_{il}\delta_{jk}$ and $\delta_{ik}\delta_{jl}$ we arrive at the 3×3 inhomogeneous system of linear equations

$$\begin{bmatrix} N_c & 1 & 1 \\ 1 & N_c & 1 \\ 1 & 1 & N_c \end{bmatrix} \begin{bmatrix} \langle \hat{A} \rangle_Y \\ \langle \hat{B} \rangle_Y \\ \langle \hat{C} \rangle_Y \end{bmatrix} = \begin{bmatrix} N_c \langle \hat{S}_{\mathbf{x}_1 \mathbf{x}_2} \hat{S}_{\mathbf{x}_3 \mathbf{x}_4} \hat{O} \rangle_Y \\ \langle \hat{Q}_{\mathbf{x}_1 \mathbf{x}_2 \mathbf{x}_3 \mathbf{x}_4} \hat{O} \rangle_Y \\ \langle \hat{R}_{\mathbf{x}_1 \mathbf{x}_2 \mathbf{x}_3 \mathbf{x}_4} \hat{O} \rangle_Y \end{bmatrix}, \quad (7.11)$$

where we have defined the operator $\hat{R}_{\mathbf{x}_1 \mathbf{x}_2 \mathbf{x}_3 \mathbf{x}_4} = (1/N_c)(V_{\mathbf{x}_1}^\dagger V_{\mathbf{x}_2})(V_{\mathbf{x}_3}^\dagger V_{\mathbf{x}_4})_{ij}$. Solving Eq. (7.11) we obtain the gauge-invariant operators

$$\langle \hat{A} \rangle_Y = \frac{N_c(N_c + 1) \langle \hat{S}_{\mathbf{x}_1 \mathbf{x}_2} \hat{S}_{\mathbf{x}_3 \mathbf{x}_4} \hat{O} \rangle_Y - \langle \hat{Q}_{\mathbf{x}_1 \mathbf{x}_2 \mathbf{x}_3 \mathbf{x}_4} \hat{O} \rangle_Y - \langle \hat{R}_{\mathbf{x}_1 \mathbf{x}_2 \mathbf{x}_3 \mathbf{x}_4} \hat{O} \rangle_Y}{(N_c + 2)(N_c - 1)}, \quad (7.12)$$

$$\langle \hat{B} \rangle_Y = \frac{(N_c + 1) \langle \hat{Q}_{\mathbf{x}_1 \mathbf{x}_2 \mathbf{x}_3 \mathbf{x}_4} \hat{O} \rangle_Y - \langle \hat{R}_{\mathbf{x}_1 \mathbf{x}_2 \mathbf{x}_3 \mathbf{x}_4} \hat{O} \rangle_Y - N_c \langle \hat{S}_{\mathbf{x}_1 \mathbf{x}_2} \hat{S}_{\mathbf{x}_3 \mathbf{x}_4} \hat{O} \rangle_Y}{(N_c + 2)(N_c - 1)}, \quad (7.13)$$

$$\langle \hat{C} \rangle_Y = \frac{(N_c + 1) \langle \hat{R}_{\mathbf{x}_1 \mathbf{x}_2 \mathbf{x}_3 \mathbf{x}_4} \hat{O} \rangle_Y - \langle \hat{Q}_{\mathbf{x}_1 \mathbf{x}_2 \mathbf{x}_3 \mathbf{x}_4} \hat{O} \rangle_Y - N_c \langle \hat{S}_{\mathbf{x}_1 \mathbf{x}_2} \hat{S}_{\mathbf{x}_3 \mathbf{x}_4} \hat{O} \rangle_Y}{(N_c + 2)(N_c - 1)}. \quad (7.14)$$

This is general and one would need to calculate separately the expectation values of the operators $\hat{S}\hat{S}\hat{O}$, $\hat{Q}\hat{O}$ and $\hat{R}\hat{O}$. Of course considerable simplifications are expected to occur in the Gaussian approximation; indeed, one finds that $\hat{S}\hat{S}\hat{O}$, $\hat{Q}\hat{O}$ and $\hat{R}\hat{O}$ are such that $\langle \hat{C} \rangle_Y$ in Eq. (7.14) vanishes and, thus, the color structure $\delta_{ik}\delta_{jl}$ does not appear any more in Eq. (7.10). Furthermore, by eliminating $\hat{R}\hat{O}$, we can simplify $\langle \hat{A} \rangle_Y$ and $\langle \hat{B} \rangle_Y$ to finally arrive at

$$\begin{aligned} \langle (V_{\mathbf{x}_1}^\dagger V_{\mathbf{x}_2})_{ij} (V_{\mathbf{x}_3}^\dagger V_{\mathbf{x}_4})_{kl} \hat{O} \rangle_Y &= \delta_{ij}\delta_{kl} \frac{N_c^2 \langle \hat{S}_{\mathbf{x}_1 \mathbf{x}_2} \hat{S}_{\mathbf{x}_3 \mathbf{x}_4} \hat{O} \rangle_Y - \langle \hat{Q}_{\mathbf{x}_1 \mathbf{x}_2 \mathbf{x}_3 \mathbf{x}_4} \hat{O} \rangle_Y}{N_c^2 - 1} \\ &\quad + \delta_{il}\delta_{jk} \frac{N_c \langle \hat{Q}_{\mathbf{x}_1 \mathbf{x}_2 \mathbf{x}_3 \mathbf{x}_4} \hat{O} \rangle_Y - N_c \langle \hat{S}_{\mathbf{x}_1 \mathbf{x}_2} \hat{S}_{\mathbf{x}_3 \mathbf{x}_4} \hat{O} \rangle_Y}{N_c^2 - 1}. \end{aligned} \quad (7.15)$$

In the large- N_c limit one can neglect the term involving the quadrupole in the first fraction and also set $N_c^2 - 1 \approx N_c^2$ in the denominators. However, one should be careful not to perform any further large- N_c approximation at this stage; a measurable quantity will involve contractions over the color indices in Eq. (7.15) and such a procedure can alter the N_c counting.

VIII. CONCLUSIONS AND PERSPECTIVES

Analytic expressions for multi-gluon correlators in the high energy limit are indispensable in order to reduce the numerical cost for obtaining the cross sections related to multi-particle production. Such expressions arise in the context of the Gaussian approximation to the JIMWLK evolution equation, and in this work we have studied the validity of such an approximation. Our results are already succinctly expressed in the last paragraph of the Introduction (Sect. I). In short, we have confirmed that the Gaussian approximation provides a quasi-exact solution and in particular we have shown that this is the case independent of the prescription used to set the scale in the argument of the running coupling.

Still, there remain a few things which could be addressed in a future work. It is important to explore how solid the Gaussian approximation is when we use more general initial conditions,

like, for example, those in [71] and we do believe that the answer to this question is positive. Furthermore, as discussed in Sect. VI, it would be interesting to check if the use of the more general expressions in the Gaussian approximation, like the one in Eq. (4.4), instead of the extrapolation of the MV model to arbitrary Y , like in Eq. (4.6), improve the accuracy in running coupling evolution. Last, but not least, one should perhaps examine how and if the approximation applies to the case of unequal rapidity correlations.

ACKNOWLEDGMENTS

G.S.'s work is supported by the Agence Nationale de la Recherche project 11-BS04-015-01. Figures 1, 2, 3, 8 and 9 were created with Jaxodraw [73, 74].

Appendix: Numerical implementation

In this Appendix, we sketch the main points of the numerical techniques used to solve the evolution equations in this paper. Most of them are common to the BK equation, that is the factorized version of Eq. (2.12), the MFA equation Eq. (5.1) and the equation of the square configuration Eq. (6.6), so we will focus on the BK equation below and comment on the other cases after.

For the integration of the right-hand side of the equation, the first step is to use the mirror symmetry along the bisector of the external dipole line x_1 , x_2 and limit the integration to the half-plane containing x_1 . In that region, we integrate in polar coordinates around x_1 and easily get

$$\int_{\mathbf{z}} \mathcal{M}_{\mathbf{x}_1 \mathbf{x}_2 \mathbf{z}} = \int_{-\infty}^{\infty} d\ell \int_{\theta_0(\ell)}^{2\pi - \theta_0(\ell)} \frac{(\mathbf{x}_1 - \mathbf{x}_2)^2}{(\mathbf{z} - \mathbf{x}_2)^2} \quad (\text{A.1})$$

where $\ell = \ln(1/(\mathbf{x}_1 - \mathbf{z})^2)$ and the bounds on the θ integration — with θ measured from the 12 axis — depend on ℓ . The radial and angular integrations are then discretised. We typically use 16 points in θ and 1440 points in ℓ with $-40 \leq \ell \leq 140$. We have checked that for all the plots presented in this paper, the discretisation in ℓ was fine enough to reach the quoted accuracy.

Then, since deep at saturation $\langle \hat{S}(r) \rangle_Y$ becomes extremely small when rapidity increases, we decided to work instead with $s(r, Y) = \ln(1/\langle \hat{S}(r) \rangle_Y)$ and all the equations are rewritten in terms of s . To achieve maximal numerical precision, terms that cancel the logarithmic ultraviolet divergence when \mathbf{z} approaches \mathbf{x}_1 are grouped.

Knowing the right-hand side of the equation, the numerical evolution in rapidity is then handled using a standard fourth-order Runge-Kutta method.

This method applies straightforwardly to the BK and MFA equations. For the equation of the square configuration, the bisector of the $(\mathbf{x}_1, \mathbf{x}_2)$ dipole goes through \mathbf{x}_4 and one may wonder about the possible ultraviolet divergence when \mathbf{z} approaches \mathbf{x}_4 . It is easy to notice that this appears under the form of the combination of BFKL kernels $\mathcal{M}_{\mathbf{x}_1 \mathbf{x}_4 \mathbf{z}} - \mathcal{M}_{\mathbf{x}_2 \mathbf{x}_4 \mathbf{z}}$, which is only linearly divergent for $\mathbf{z} \rightarrow \mathbf{x}_4$, multiplied by a combination of the dipole amplitude $S(\mathbf{z})$ that vanishes when $\mathbf{z} \rightarrow \mathbf{x}_4$, giving an overall smooth behaviour.

Finally, let us notice that the formulation of the evolution in terms of $s(r, Y) = \ln(1/\langle \hat{S}(r) \rangle_Y)$ also has its limitations if Y becomes too large. This is because, in order to obtain the full asymptotic geometric scaling behaviour, one needs to describe correctly the dilute tail over the whole geometric scaling region. Since this extends to smaller and smaller $\langle \hat{T}(r) \rangle_Y$, with $\langle \hat{T}(r) \rangle_Y \approx s(r, Y)$, when rapidity increases, a better precision in the dilute region is obtained by working with $\ln(1/\langle \hat{T}(r) \rangle_Y)$. This can be combined with the dense region by using a mixed variable $X(r, Y) = \max\{\ln(2/\langle \hat{S}(r) \rangle_Y), \ln(2/\langle \hat{T}(r) \rangle_Y)\}$. This can be implemented using the techniques above and keeping track of the threshold ℓ_0 where the transition between $X = \ln(2/\langle \hat{S}(r) \rangle_Y)$ and $X = \ln(2/\langle \hat{T}(r) \rangle_Y)$ occurs, *i.e.* where $\langle \hat{S}(\ell_0) \rangle_Y = \langle \hat{T}(\ell_0) \rangle_Y = 1/2$. It is this method that we have developed to verify the Levin-Tuchin formula.

-
- [1] BRAHMS Collaboration, I. Arsene *et al.*, Phys.Rev.Lett. **93**, 242303 (2004), [nucl-ex/0403005].
 - [2] STAR Collaboration, J. Adams *et al.*, Phys.Rev.Lett. **97**, 152302 (2006), [nucl-ex/0602011].
 - [3] STAR Collaboration, E. Braidot, Nucl.Phys. **A854**, 168 (2011), [1008.3989].
 - [4] PHENIX Collaboration, A. Adare *et al.*, Phys.Rev.Lett. **107**, 172301 (2011), [1105.5112].
 - [5] D. Kharzeev, Y. V. Kovchegov and K. Tuchin, Phys.Rev. **D68**, 094013 (2003), [hep-ph/0307037].
 - [6] J. L. Albacete, N. Armesto, A. Kovner, C. A. Salgado and U. A. Wiedemann, Phys.Rev.Lett. **92**, 082001 (2004), [hep-ph/0307179].
 - [7] J. P. Blaizot, F. Gelis and R. Venugopalan, Nucl.Phys. **A743**, 13 (2004), [hep-ph/0402256].
 - [8] E. Iancu, K. Itakura and D. Triantafyllopoulos, Nucl.Phys. **A742**, 182 (2004), [hep-ph/0403103].
 - [9] J. L. Albacete and C. Marquet, Phys.Lett. **B687**, 174 (2010), [1001.1378].
 - [10] T. Altinoluk and A. Kovner, Phys.Rev. **D83**, 105004 (2011), [1102.5327].
 - [11] J. Jalilian-Marian and A. H. Rezaeian, Phys.Rev. **D85**, 014017 (2012), [1110.2810].
 - [12] G. A. Chirilli, B.-W. Xiao and F. Yuan, Phys.Rev.Lett. **108**, 122301 (2012), [1112.1061].
 - [13] P. Tribedy and R. Venugopalan, Phys.Lett. **B710**, 125 (2012), [1112.2445].
 - [14] A. Mueller and S. Munier, 1206.1333.
 - [15] J. L. Albacete, A. Dumitru, H. Fujii and Y. Nara, Nucl.Phys. **A897**, 1 (2013), [1209.2001].
 - [16] A. H. Rezaeian, 1210.2385.
 - [17] J. Jalilian-Marian and Y. V. Kovchegov, Phys. Rev. **D70**, 114017 (2004), [hep-ph/0405266].
 - [18] C. Marquet, Nucl. Phys. **A796**, 41 (2007), [0708.0231].
 - [19] K. Tuchin, Nucl.Phys. **A846**, 83 (2010), [0912.5479].
 - [20] J. L. Albacete and C. Marquet, Phys. Rev. Lett. **105**, 162301 (2010), [1005.4065].
 - [21] A. Stasto, B.-W. Xiao and F. Yuan, Phys.Lett. **B716**, 430 (2012), [1109.1817].
 - [22] T. Lappi and H. Mantysaari, 1209.2853.
 - [23] E. Iancu, A. Leonidov and L. McLerran, hep-ph/0202270.
 - [24] Y. V. Kovchegov and K. Tuchin, Phys.Rev. **D65**, 074026 (2002), [hep-ph/0111362].
 - [25] A. Kovner and M. Lublinsky, JHEP **0611**, 083 (2006), [hep-ph/0609227].
 - [26] F. Gelis, T. Lappi and R. Venugopalan, Phys.Rev. **D79**, 094017 (2009), [0810.4829].
 - [27] K. Dusling, F. Gelis, T. Lappi and R. Venugopalan, Nucl.Phys. **A836**, 159 (2010), [0911.2720].
 - [28] Y. V. Kovchegov and D. E. Wertepny, 1212.1195.
 - [29] F. Dominguez, C. Marquet, A. M. Stasto and B.-W. Xiao, 1210.1141.
 - [30] L. D. McLerran and R. Venugopalan, Phys. Rev. **D49**, 2233 (1994), [hep-ph/9309289].
 - [31] L. D. McLerran and R. Venugopalan, Phys. Rev. **D49**, 3352 (1994), [hep-ph/9311205].

- [32] J. P. Blaizot, F. Gelis and R. Venugopalan, Nucl. Phys. **A743**, 57 (2004), [hep-ph/0402257].
- [33] F. Dominguez, C. Marquet, B.-W. Xiao and F. Yuan, Phys. Rev. **D83**, 105005 (2011), [1101.0715].
- [34] J. Jalilian-Marian, A. Kovner, A. Leonidov and H. Weigert, Nucl. Phys. **B504**, 415 (1997), [hep-ph/9701284].
- [35] J. Jalilian-Marian, A. Kovner, A. Leonidov and H. Weigert, Phys. Rev. **D59**, 014014 (1998), [hep-ph/9706377].
- [36] H. Weigert, Nucl. Phys. **A703**, 823 (2002), [hep-ph/0004044].
- [37] E. Iancu, A. Leonidov and L. D. McLerran, Nucl. Phys. **A692**, 583 (2001), [hep-ph/0011241].
- [38] E. Iancu, A. Leonidov and L. D. McLerran, Phys. Lett. **B510**, 133 (2001), [hep-ph/0102009].
- [39] J.-P. Blaizot, E. Iancu and H. Weigert, Nucl. Phys. **A713**, 441 (2003), [hep-ph/0206279].
- [40] A. Dumitru, J. Jalilian-Marian, T. Lappi, B. Schenke and R. Venugopalan, Phys.Lett. **B706**, 219 (2011), [1108.4764].
- [41] E. Iancu and D. Triantafyllopoulos, JHEP **1111**, 105 (2011), [1109.0302].
- [42] E. Iancu and D. Triantafyllopoulos, JHEP **1204**, 025 (2012), [1112.1104].
- [43] E. Levin and K. Tuchin, Nucl. Phys. **B573**, 833 (2000), [hep-ph/9908317].
- [44] A. H. Mueller and G. Salam, Nucl.Phys. **B475**, 293 (1996), [hep-ph/9605302].
- [45] E. Iancu and L. D. McLerran, Phys. Lett. **B510**, 145 (2001), [hep-ph/0103032].
- [46] A. H. Mueller, Nucl. Phys. **B643**, 501 (2002), [hep-ph/0206216].
- [47] E. Iancu and A. H. Mueller, Nucl. Phys. **A730**, 494 (2004), [hep-ph/0309276].
- [48] I. Balitsky, Nucl. Phys. **B463**, 99 (1996), [hep-ph/9509348].
- [49] Y. V. Kovchegov, Phys. Rev. **D60**, 034008 (1999), [hep-ph/9901281].
- [50] Y. Hatta, E. Iancu, K. Itakura and L. McLerran, Nucl. Phys. **A760**, 172 (2005), [hep-ph/0501171].
- [51] A. H. Mueller, Nucl.Phys. **B415**, 373 (1994).
- [52] I. Balitsky, hep-ph/0101042.
- [53] D. N. Triantafyllopoulos, Acta Phys. Polon. **B36**, 3593 (2005), [hep-ph/0511226].
- [54] K. Rummukainen and H. Weigert, Nucl. Phys. **A739**, 183 (2004), [hep-ph/0309306].
- [55] T. Lappi, Phys.Lett. **B703**, 325 (2011), [1105.5511].
- [56] A. H. Mueller and D. N. Triantafyllopoulos, Nucl. Phys. **B640**, 331 (2002), [hep-ph/0205167].
- [57] S. Munier and R. B. Peschanski, Phys.Rev. **D69**, 034008 (2004), [hep-ph/0310357].
- [58] L. V. Gribov, E. M. Levin and M. G. Ryskin, Phys. Rept. **100**, 1 (1983).
- [59] E. Kuraev, L. Lipatov and V. S. Fadin, Sov.Phys.JETP **45**, 199 (1977).
- [60] I. Balitsky and L. Lipatov, Sov.J.Nucl.Phys. **28**, 822 (1978).
- [61] A. M. Stasto, K. J. Golec-Biernat and J. Kwiecinski, Phys. Rev. Lett. **86**, 596 (2001), [hep-ph/0007192].
- [62] E. Iancu, K. Itakura and L. McLerran, Nucl. Phys. **A708**, 327 (2002), [hep-ph/0203137].
- [63] S. Munier and R. B. Peschanski, Phys. Rev. Lett. **91**, 232001 (2003), [hep-ph/0309177].
- [64] Y. V. Kovchegov and H. Weigert, Nucl.Phys. **A784**, 188 (2007), [hep-ph/0609090].
- [65] I. Balitsky, Phys.Rev. **D75**, 014001 (2007), [hep-ph/0609105].
- [66] I. Balitsky and G. A. Chirilli, Phys.Rev. **D77**, 014019 (2008), [0710.4330].
- [67] D. N. Triantafyllopoulos, Nucl. Phys. **B648**, 293 (2003), [hep-ph/0209121].
- [68] G. Beuf, 1008.0498.
- [69] E. Iancu, K. Itakura and L. McLerran, Nucl. Phys. **A724**, 181 (2003), [hep-ph/0212123].
- [70] Y. V. Kovchegov, J. Kuokkanen, K. Rummukainen and H. Weigert, Nucl. Phys. **A823**, 47 (2009), [0812.3238].
- [71] A. Dumitru and E. Petreska, Nucl.Phys. **A879**, 59 (2012), [1112.4760].
- [72] J. Berger and A. M. Stasto, Phys.Rev. **D84**, 094022 (2011), [1106.5740].
- [73] D. Binosi and L. Theussl, Comput. Phys. Commun. **161**, 76 (2004), [hep-ph/0309015].
- [74] D. Binosi, J. Collins, C. Kaufhold and L. Theussl, Comput.Phys.Comm. **180**, 1709 (2009),

[0811.4113].